Geological Society of America
Special Paper 403
2006

Non-ultrahigh-pressure unit bordering the Sulu ultrahigh-pressure terrane, eastern China: Transformation of Proterozoic granulite and gabbro to garnet amphibolite

Ru Y. Zhang
Juhn G. Liou
Tatsuki Tsujimori
Department of Geological and Environmental Sciences, Stanford University, Stanford, California 94305, USA
Shigenori Maruyama
Department of Earth and Planetary Sciences, Tokyo Institute of Technology, Tokyo, Japan

ABSTRACT

The Haiyangsuo area of the NE Sulu ultrahigh-pressure terrane, eastern China, consists of gneisses with minor granulite and amphibolite layers, metagabbros, and granitic dikes. The peak-stage assemblages of the granulites (garnet + orthopyroxene + clinopyroxene + plagioclase ± pargasite ± biotite ± quartz) formed at >750 °C and 9–11 kbar and were overprinted by amphibolite-facies phases characterized by well-developed corona layers of │garnet│amphibolite + quartz│at contacts between plagioclase and clinopyroxene or orthopyroxene, as well as by the exsolution of (orthopyroxene + ilmenite + amphibole) from clinopyroxene. These textures indicate a near-isobaric cooling history of the granulite-bearing gneiss terrane. The metagabbro preserves a relict igneous assemblage (orthopyroxene + clinopyroxene + plagioclase + pargasite ± ilmenite ± quartz) in its core, but in its margins has a metamorphic corona texture similar to the granulite that formed at ~600–700 °C and 7–10 kbar. Sensitive high-resolution ion microprobe (SHRIMP) U-Pb dating of zircons indicates that the protolith age of the garnet-biotite gneiss is older than 2500 Ma, whereas the granulite-facies metamorphism (the first regional metamorphic event) occurred at 1846 ± 26 Ma. Gabbro intrusion took place at 1734 ± 5 Ma, and the formation of amphibolite assemblages in both metagabbro and granulite occurred at ca. 340–370 Ma. Both gneiss and metagabbro were intruded by granitic dikes, with one dated at 158 ± 3 Ma. These data, together with a lack of eclogitic assemblages, suggest that this granulite-amphibolite–facies complex is exotic relative to the Triassic Sulu high-pressure–ultrahigh-pressure terrane; juxtaposition took place in Jurassic time.

Keywords: non-ultrahigh-pressure unit, Sulu UHP terrane, gabbro, garnet amphibolite, geochronology.

Zhang, R.Y., Liou, J.G., Tsujimori, T., and Maruyama, S., 2006, Non-ultrahigh-pressure unit bordering the Sulu ultrahigh-pressure terrane, eastern China: Transformation of Proterozoic granulite and gabbro to garnet amphibolite, *in* Hacker, B.R., McClelland, W.C., and Liou, J.G., eds., Ultrahigh-pressure metamorphism: Deep continental subduction: Geological Society of America Special Paper 403, p. 169–206, doi: 10.1130/2006.2403(10).

INTRODUCTION

Since coesite was first identified in Donghai eclogite in 1990 (Hirajima et al., 1990), this phase has been reported as inclusions in eclogitic garnet, omphacite, kyanite, and epidote and gneissic zircons in many Sulu ultrahigh-pressure (UHP) rocks (Fig. 1). Hence, in situ Triassic UHP metamorphism has been considered a characteristic of the subducted supracrustal rocks of the northern Yangtze craton (Zhang et al., 1995; Wallis et al., 1999; Ye et al. 2000; Liu et al. 2004a, 2004b, 2005). However, we recently identified a non-UHP unit composed of granulite-bearing amphibolite-facies gneiss with Proterozoic gabbroic bodies larger than 15 km^2 (Fig. 2) at Haiyangsuo, along the southern coast of the northeastern Shandong Peninsula. The gabbroic rock has been considered an important component of the "Jaiodong Proterozoic ophiolite sequence" (Wang et al., 1995), which consists of widely separated blocks of ultramafic rock, chert and metavolcanic rocks, all of which are significantly deformed and recrystallized ophiolitic rocks. Subsequently, Ye et al. (1999) described granulite relics (Opx + Cpx + Grt + Pl + Amp; abbreviations after Kretz, 1983) within amphibolite displaying garnet coronae between plagioclase and mafic minerals. They named rocks with the assemblage Grt_2 + Cpx_2 (Omp/Di) + Pl_2 (Ab) + Zo + Hbl_2 + Ky + Rt "transitional eclogite." They further suggested that the Haiyangsuo area is similar to the "cold eclogite" belt in Dabie, and represents a southern unit of the Sulu UHP metamorphic belt. As granulite-facies protoliths are rare for Dabie-Sulu UHP rocks, their findings motivated us to investigate the lithology, pressure-temperature (*P-T*) paths, and geochronology of various Haiyangsuo rocks. We conclude that the Haiyangsuo area is exotic with respect to the Sulu high-pressure–ultrahigh-pressure rocks; the two must be separated by a tectonic boundary, but the intervening area is covered by Quaternary sediments.

GEOLOGICAL OUTLINE

The Sulu metamorphic terrane is an eastern extension of the Triassic Qinling-Dabie collision zone between the Yangtze and Sino-Korean cratons, and consists of an UHP belt to the

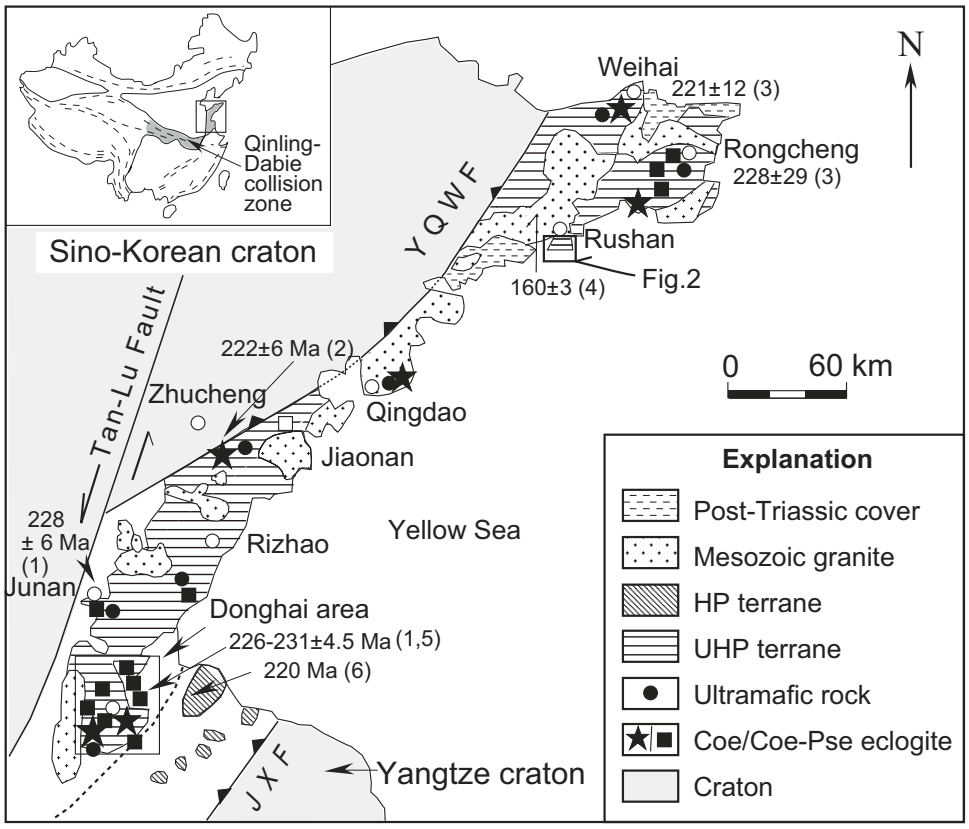

Figure 1. Simplified geological map of the study area and the Sulu region, showing major tectonic units and distribution of coesite (Coe)-bearing and coesite pseudomorph (Coe pse)–bearing eclogites. Metamorphic ages: (1) Sm-Nd ages of eclogite after Li et al. (1993), (2) Sm-Nd isochron age after Han et al. (1993); (3) zircon sensitive high-resolution ion microprobe (SHRIMP) U-Pb age for peridotite (Weihai) and eclogite (Rongcheng) after Yang et al. (2003); (4) monazite SHRIMP U-Pb age of Rushan granite from Hu et al. (2004); (5) zircon SHRIMP U-Pb age of CCSD-PP2 gneiss at Donghai after Liu et al. (2004b), and (6) $^{40}Ar/^{39}Ar$ plateau age of white mica for high-pressure belt mica and quartz schist after Cong et al. (1992). Abbreviations: JXF—Jiashan-Xianshui fault; YQWF—Yantai-Qingdao-Wulian fault; HP—high pressure; UHP—ultrahigh pressure.

north and a high-pressure belt to the south (Fig. 1; Zhang et al., 1995); the boundary in the vicinity of Donghai has recently been confirmed by a systematic study of mineral inclusions in zircons and is characterized by a mylonitic zone (e.g., Liu et al., 2004a). The UHP belt is composed of gneiss, amphibolite, and small amount of marble and quartzite. Widespread coesite-bearing eclogites occur as lenses and layers in gneiss, marble, and ultramafic rocks. Most of the UHP metamorphic garnet peridotites occur as block in gneiss. Most of the protolith ages of the eclogites and the country-rock gneisses range from 600 to 800 Ma, and UHP metamorphic ages are 220–240 Ma (Fig. 1; Li et al., 1993; Ames et al., 1996; Liu et al., 2004b, 2005; Leech et al., this volume; Webb et al., this volume; Hacker et al., 2006). The high-pressure belt in Sulu consists of gneiss, mica schist, kyanite-bearing mica schist, kyanite-topaz–bearing quartzite, marble, phosphatic rocks, and minor blueschist (Zhang and Kang, 1989); no eclogite has been found. These UHP and high-pressure belts of the Sulu terrane are intruded by Mesozoic granites and are unconformably overlain by Jurassic–Cretaceous volcanic-sedimentary cover sequences.

FIELD INVESTIGATION

The Haiyangsuo area in the northeastern Sulu UHP terrane, along the coast of southern Rushan county (Fig. 1), consists of three lithological units: (1) gneiss with granulite lenses and amphibolite layers, (2) metamorphosed gabbro intrusions, and (3) granitic dikes. Units 1 and 2 are dominant and display several stages of deformation and metamorphic recrystallization. Widespread gabbro bodies of ~15 km^2 (Fig. 2) exhibit clear crosscutting relationships with their host gneiss (Fig. 3); some show concordant contacts (e.g., gabbro intruded along the foliation of the gneiss). Some gneisses and late granitic dikes show a mylonitic foliation that wraps around the margins of some of the mafic bodies (Fig. 4A). A fine-grained, pale-red coronal metagabbro occurs in the cores of some of the metagabbro bodies (Fig. 4B); it is easy to misidentify as eclogite. Toward the margins of the mafic bodies, the rock becomes dark green due to amphibolite-facies recrystallization; the boundary between the outer amphibolite and inner coronal metagabbro is gradational. The red metagabbro core varies in size; most are 1–10 m in diameter. Young granitic dikes cut across all lithologic units, including the gneiss and metagabbro (Fig. 3).

PETROGRAPHY

Unit 1: Gneiss with Granulite Lens and Amphibolite Layer

Relics of granulite occur as meter-scale lenses or layers in the gneiss rock; they exhibit various extents of retrogression to garnet amphibolite. In our collections, three granulite-facies mineral assemblages were identified at different locations. (1) Biotite-bearing granulite consists of coarse-grained garnet, clinopyroxene, orthopyroxene, plagioclase, and quartz with

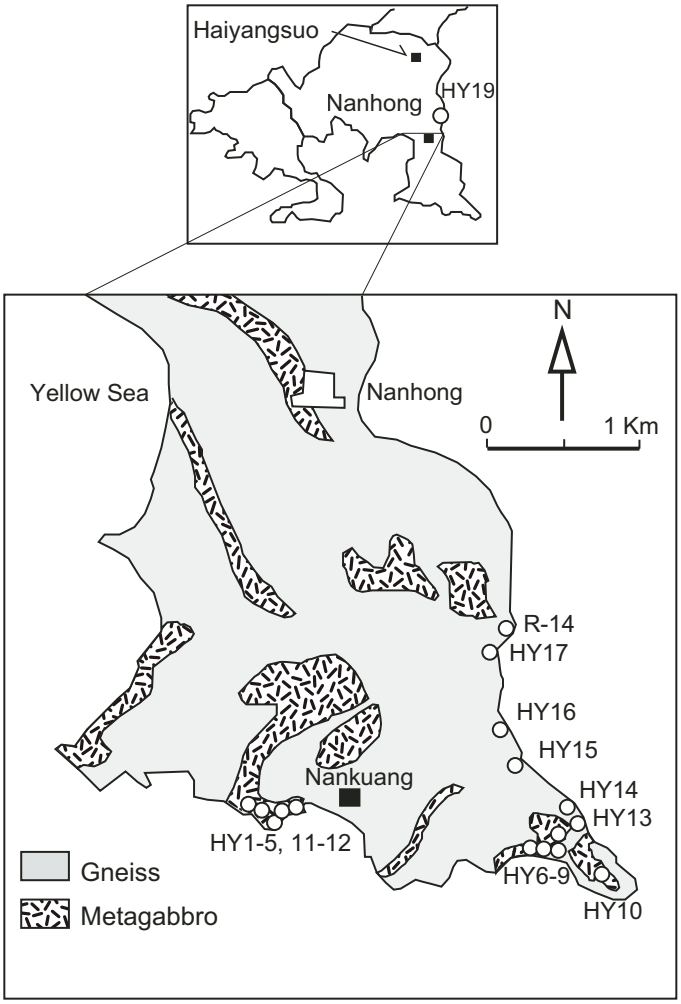

Figure 2. Schematic geologic map of the Haiyangsuo area showing distribution of metagabbro in gneissic rocks and sample locations.

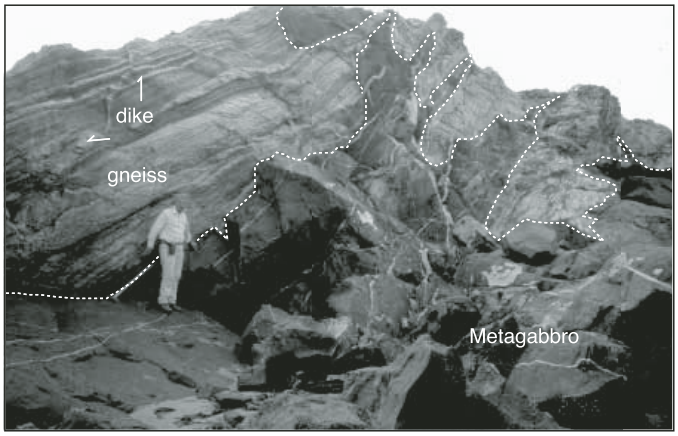

Figure 3. Field view showing relationship of various rock types. Gabbro intrusives crosscut gneiss, and thin granitic dikes either are along foliation or crosscut both gabbro and gneiss.

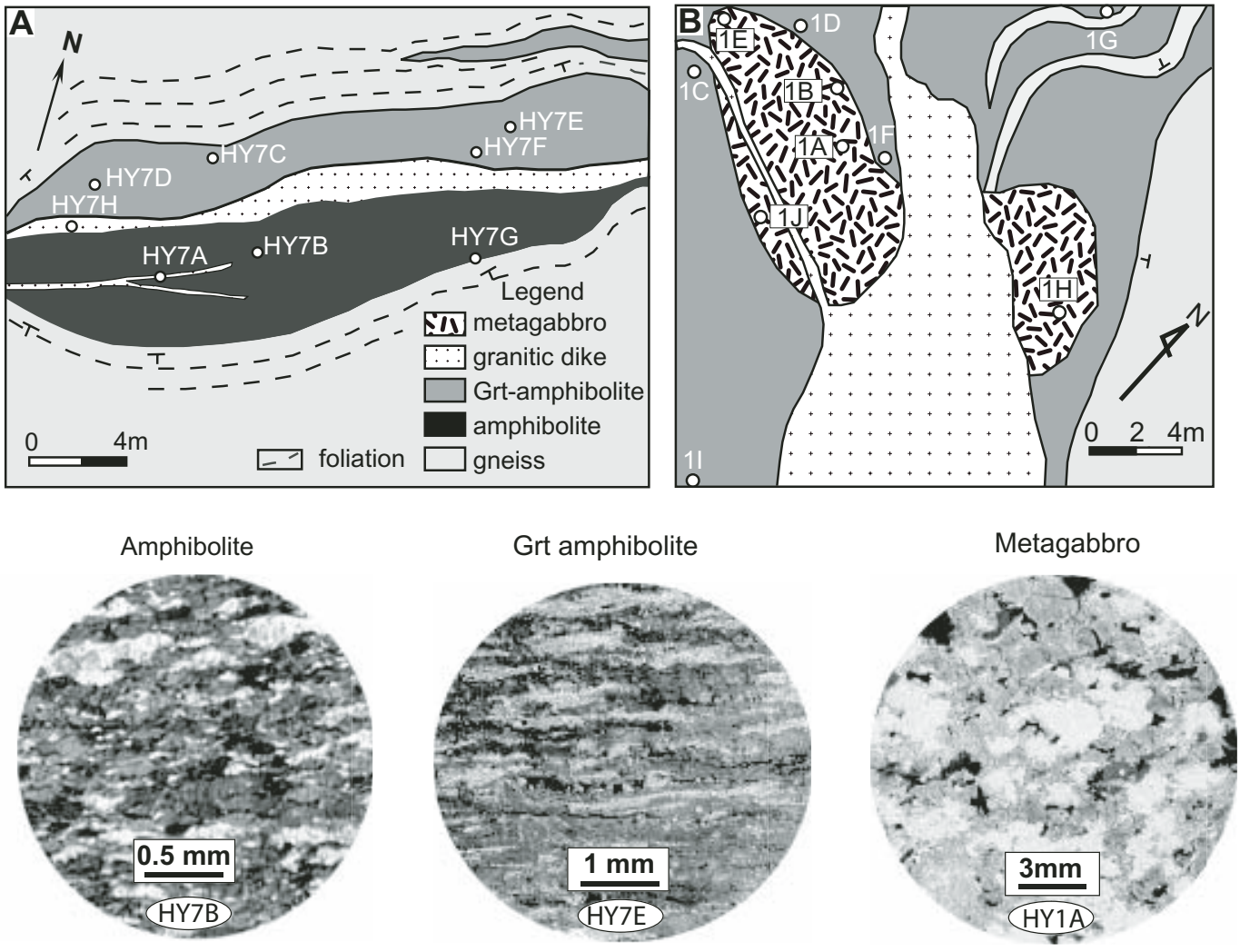

Figure 4. Geological mapping of two outcrops and scanning images of three thin sections for representative samples in the Haiyangsuo area. (A) Gneiss wraps around garnet-free (e.g., HY7B) and garnet-bearing amphibolite (e.g., HY7E). Very fine-grained garnet amphibolite with gabbroic protolith shows strong deformation and distribution of coronic garnets along foliation (HY7E). (B) A small gabbro body is intruded by a granitic dike; metamorphosed gabbro (e.g., HY1A) occurs in the core of the gabbro body and changes to garnet amphibolite at the margin.

minor biotite and ilmenite (Fig. 5A). Most garnets are ~4 mm across. Most pyroxenes of 1–3 mm show undulatory extinction and exsolution (sample 03-R14). Biotite occurs as relict coarse-grained blocky crystals or as secondary fine-grained scaly aggregates. (2) Pargasite-bearing granulite (Fig. 5B) contains Grt + Opx + Cpx + Pl + Prg + Rt/Ilm assemblages; garnet is 0.5–1.75 mm across, and the two pyroxenes are 0.3–1 mm in size; amphibole is pale yellow–brown and varies in abundance from 3 to 15 vol% (sample 12A-B). (3) Garnet pyroxenite consists of Grt, Opx, Cpx, and minor Ilm (samples 15A-D). Round garnet is the most abundant phase (60–70 vol%), 0.5–5 mm across, occurs as isolated grains and patches composed of garnets of variable size, and contains ilmenite inclusions. Pyroxene is an interstitial phase between garnets and is smaller (1–2 mm) than most garnets. Porphyroblastic garnet, 2 cm across in some pyroxenites (e.g., HY15E), is set in a finer matrix of Grt, Opx, Cpx, and ilmenite, and contains abundant ilmenite lamellae (Fig. 5C).

All granulites are weakly deformed and granoblastic. Clinopyroxenes contain submicron exsolved phases, such as Opx + Ilm + Amp (HY12B; Fig. 5D) or Ilm + rare earth element (REE)-bearing epidote (03-R14). The garnet-amphibolite–facies overprinting is characterized by the formation of fine-grained garnet corona along the contacts between plagioclase and mafic phases; the common replacements are green Amp ± Qtz after Cpx, cummingtonite or calcic amphibole ± Qtz after orthopyroxene, Pl_2 + Zo after Pl_1, and titanite after ilmenite. Zoisite of various sizes occurs as prisms or laths within pseudomorphs after the primary plagioclase. Fine-grained (0.05–0.1 mm) garnet coronas are common between plagioclase and pyroxene, but diminish to small thicknesses at boundaries

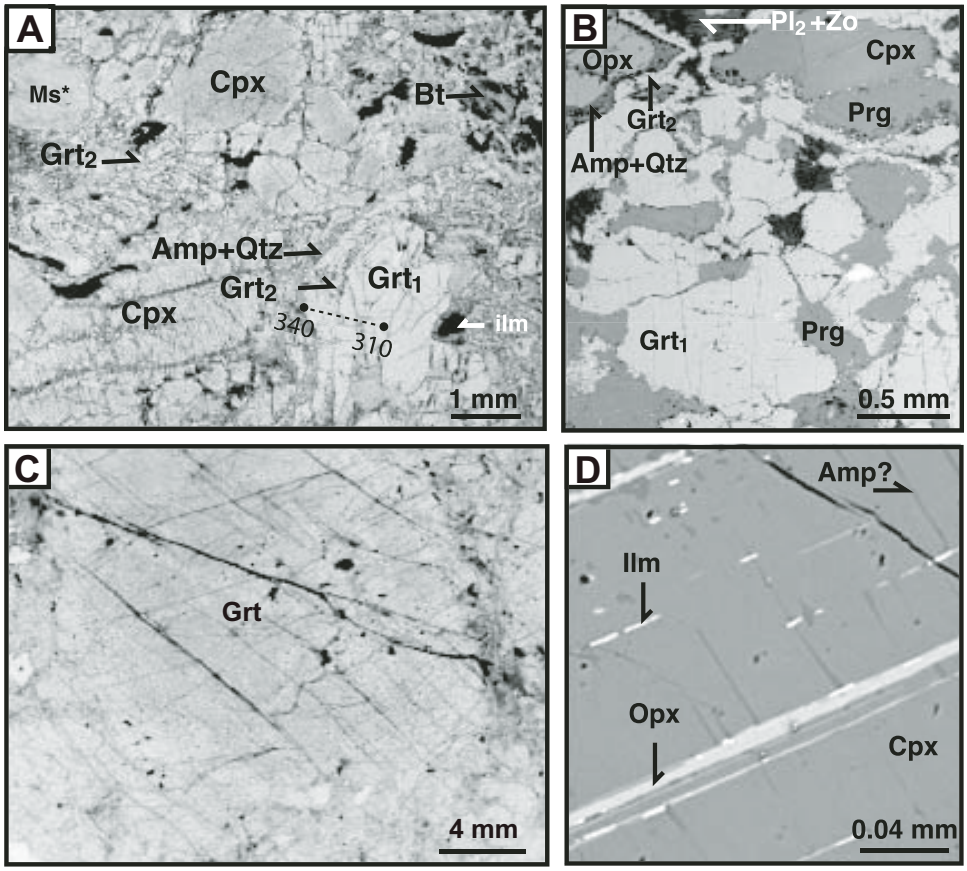

Figure 5. (A) Photomicrograph showing mineral assemblage and texture of granulite (03-R14) (plane light). In sample 03-R14, orthopyroxene is totally replaced by Amp + Qtz and coarse-grained garnet (Grt_1) is rimed by fine-grained garnets (Grt_2); fine-grained garnet coronas separate plagioclase from clinopyroxene. Ms*—white mica after plagioclase. Dashed line and number—probe analyses. (B) Backscattered-electron image (BSE) showing pargasite-bearing granulite (HY12B) with corona texture. (C) Photomicrograph of garnet pyroxenite (HY15E) showing porphyroblastic texture (plane light). (D) Exsolved lamellae of Opx, Ilm, and Amp in clinopyroxene (BSE); Amp lamellae are too thin for microanalysis. Abbreviations are after Kretz (1983).

between coarse-grained garnet (Grt_1) and pyroxene. Three corona mineral assemblages were identified: (1) Cpx (or Opx)|Amp + Qtz|Grt|Pl (Fig. 6A–B), (2) Cpx|Grt|Pl (Fig. 6C), and (3) Grt_1|Grt_2|Amp + Qtz|Cpx (Fig. 5A). In addition, some recrystallized fine-grained Cpx|Pl|Grt corona-like domains were found in plagioclase (Figs. 6D and 7).

Gneisses with distinct compositional layers include garnet-free, garnet-bearing, and quartz-rich paragneiss, orthogneiss, and mafic amphibolite. A representative sample of granitic gneiss (sample HY3) is composed of perthite, antiperthite, and quartz with no mafic minerals; it is mylonitic. Porphyroclasts (1–2 mm in size) of feldspar are set in a fine-grained matrix of fine-grained feldspar and quartz, with the minimum grain size <10 μm. Some felsic gneisses (e.g., sample HY5E) contain additional ~5 vol% amphibole; plagioclase includes abundant fine laths of zoisite and minor epidote. Sample HY17A is a garnet-rich (>40 vol%) gneiss composed of coarse, 1–6 mm garnet in a fine-grained (0.05–1 mm) matrix of pale green pargasite, colorless cummingtonite, quartz, and minor plagioclase; biotite and garnet-bearing gneisses are also common.

Most of the dark layers in the gneiss are unmylonitized Pl + Hbl ± Grt + Ttn ± Ep ± Qtz amphibolites. A foliated amphibolite (sample HY7B) consists of 90 vol% amphibole, plagioclase, and very minor titanite; the amphiboles are idioblastic and have a uniform grain size of 0.3–0.4 mm. Fine-grained titanite aggregates occur along the foliation. Garnet amphibolite (sample HY 19A) with a granoblastic texture consists of 0.5–0.8 mm euhedral garnet, 0.2–0.6 mm amphibole, plagioclase, minor quartz (~4%), and titanite.

Unit 2: Metagabbro

Gabbroic intrusive rocks exhibit various extents of amphibolite-facies recrystallization. Incipiently metamorphosed gabbro preserves intrusive relationships in its central parts and grades progressively outward to garnet amphibolite at the

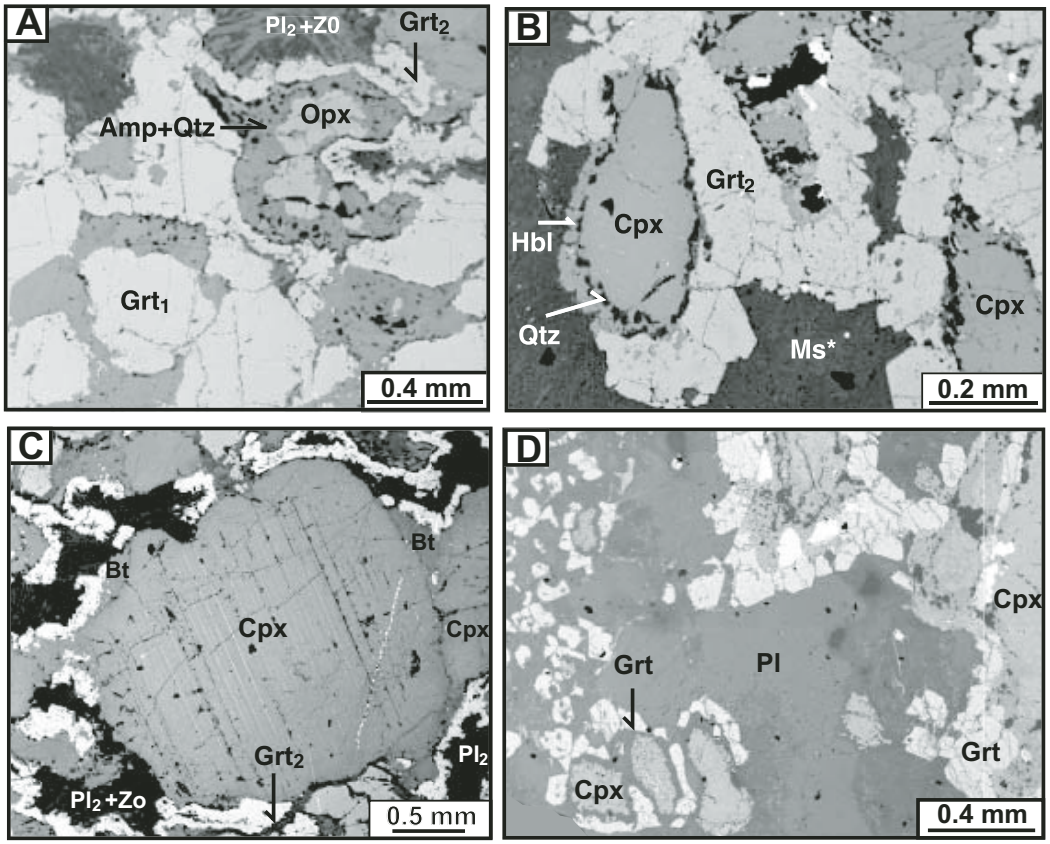

Figure 6. Backscattered-electron images showing representative corona mineral sequences of granulite (HY12B and 03-R14) and metagabbro (HY1E): Opx (or Cpx)|Amp + Qtz|Grt|Pl (A: HY12B and B: 03-R14); Cpx |Grt| Pl (C: HY12B). Small domains of Cpx (multicrystal)-Pl-Grt occur in plagioclase (D: HY1E). Abbreviations are after Kretz (1983).

margins. Coronal metagabbro in the center contains relict 0.5–1.5 mm igneous minerals, Opx + Cpx + Pl + Amp + Ilm ± Qtz (Fig. 7), some clinopyroxene, and amphibole crystals are up to 3 mm across. Plagioclase shows albite twining and only rare to minor replacement by fine-grained neoblastic anorthite, zoisite, and kyanite. Greenish clinopyroxene and pale-brown orthopyroxene contain exsolution lamellae; orthopyroxene shows greater extents of amphibole replacement than clinopyroxene. Igneous amphibole (Amp_1) shows strong pale yellowish-brown to dark yellow-green pleochroism. Ilmenite is an interstitial phase and rimmed by fine-grained titanite. The distinctive petrographic feature of the metagabbro is the presence of reaction rims separating primary orthopyroxene and clinopyroxene from plagioclase; reaction rims also occur around igneous amphibole and ilmenite. The common mineral sequences of corona layers between clinopyroxenes and plagioclase are Cpx (or Opx)|Amp_2 + Qtz|Grt|Pl_2 with zoisite and kyanite needles, or Opx|Amp_2 + Qtz + Di|Ab|Grt|Pl_2 with zoisite and kyanite needles (e.g., HY12G; Fig. 8). Rare garnet lamellae occur in clinopyroxene. In addition, some plagioclase contains isolated, 0.15–0.30-mm-diameter domains composed of clinopyroxene aggregates ± tiny Amp rimmed by Pl and then coronitic garnet (Fig. 6D; HY1E). With increasing recrystallization, the coronal metagabbro is transformed into garnet amphibolite.

The garnet amphibolite is developed at the margin of the intrusions where orthopyroxene has disappeared; only minor clinopyroxene relics are preserved. In weakly recrystallized garnet amphibolite (e.g., HY1F, HY11A, HY11B), fine-grained amphibole replaces pyroxene, long prismatic zoisite/epidote crystals form in Pl_2, and garnet corona texture is well preserved. Some garnet amphibolites are strongly deformed, with oriented Pl_2 and garnet coronas. With advanced recrystallization, garnet (~0.4 mm), hornblende (0.2–0.5 mm), and zoisite (up to 0.3 mm) coarsen (HY1C, HY1I and HY7E), and the coronal texture is no longer apparent (Fig. 4A). Mafic dikes within the gneiss were also metamorphosed at amphibolite-facies conditions. For example, sample HY19B is composed of 90 vol% amphibole, subordinate plagioclase, quartz, and very minor garnet and zoisite.

Unit 3: Felsic Dikes

Felsic dikes of various stages are abundant and cut across both gneiss and metagabbro. As these dikes are not the focus of

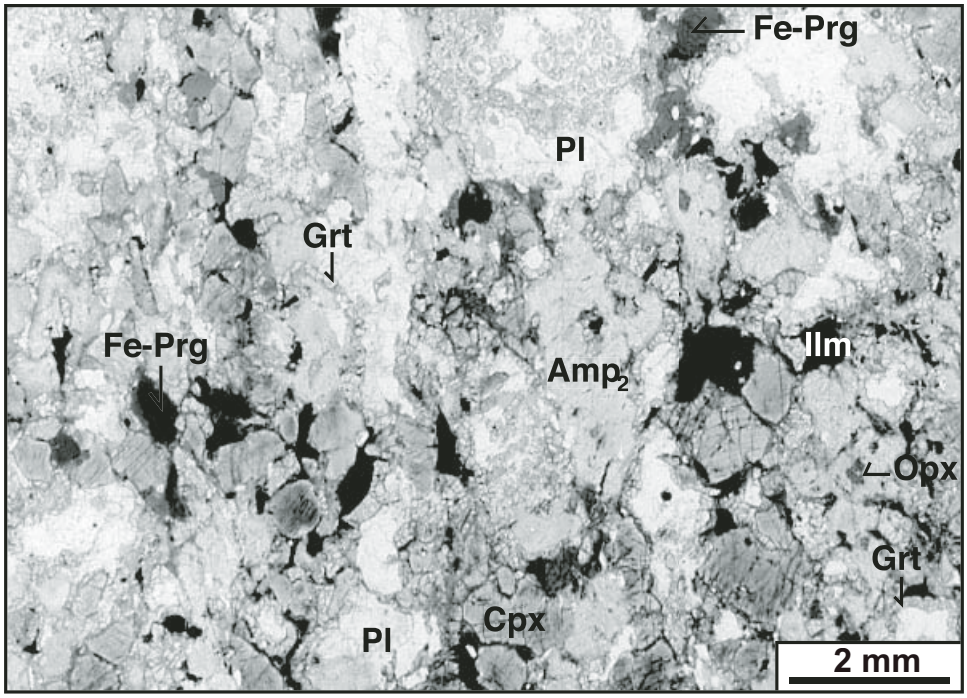

Figure 7. Photomicrograph of a metagabbro thin section (HY1E) showing assemblage (Prg + Opx + Cpx + Pl + Ilm) and texture. Only minor relict Opx is preserved; fine-grained garnet coronas occur at the contacts of pyroxenes and plagioclase. Abbreviations are after Kretz (1983).

this manuscript, we discuss only a few examples. The dikes are medium to coarse grained; some are pegmatitic. They (e.g., HY7A and HY7H) show a pronounced mylonitic texture. Porphyroclasts of plagioclase, rare microcline, quartz, and their aggregates, ranging from 0.2 to 2 mm constitute 40%–50% of the rock. These porphyroclasts are wrapped by thin layers of fine-grained, 50 μm quartz, minor white mica (±biotite ± epidote), and <10 μm quartz and feldspar. Some plagioclase porphyroclasts preserve compositional zoning and polysynthetic twinning. Minor garnets also occur in the matrix.

ZIRCON U-PB SHRIMP DATING OF GRANULITE

Few geochronologic studies of amphibolite and dikes have been carried out in Haiyangsuo. A less well-constrained (only 4 analyses) U-Pb upper intercept of 1784 ± 11 Ma and a lower intercept of 448 ± 13 Ma were obtained for the Haiyangsuo garnet amphibolite by Li et al. (1994). U-Pb sensitive high-resolution ion microprobe (SHRIMP) dating of a strongly deformed K-feldspar-rich dike from Haiyangsuo was recently reported by Wallis et al. (2005). Seven SHRIMP U-Th-Pb analyses of zircon yield a wide $^{208}Pb/^{238}U$ age range of 155.2–755.7 Ma; these analyses in the Tera-Wasserburg concordia diagram could not yield a meaningful weighted mean $^{206}Pb/^{238}U$ age or define a regression trend. In the present study, zircon separates from one granulite sample (03-R14, see description herein) were dated by the SHRIMP U-Pb method. The U-Pb SHRIMP dating results of gneiss, metagabbro, amphibolite, and granitic dike by Chu (2005) are also described.

Analytical Method

U-Th-Pb analyses were performed with the SHRIMP-RG (reverse geometry) in the Stanford–U.S. Geological Survey cooperative ion microprobe facility. Instrumental conditions and data acquisition were similar to the procedures described by Williams (1998). Analytical spots ~30 μm in diameter were sputtered using an ~5 nA O^{2-} primary beam. The data were collected in sets of 5 scans through 9 mass spectra. The primary beam was rastered across the analytical spot for 120 s before analysis to reduce surficial common Pb resulting from sample preparation and Au coating. Concentration data were calibrated against CZ3 zircon (550 ppm U), and isotope ratios were calibrated against R33 (419 Ma, John Aleinikoff, 2002, personal commun.). Data reduction followed Williams (1998) and utilized Squid (Ludwig, 2001). Isoplot 3 (Ludwig, 2003) was used to calculate all ages, which are reported here at the 95% confidence level.

Results

Most zircons were rounded, ranged in size from 50 to 150 μm, and showed weak cathodoluminescence (CL) response without obvious cores (Fig. 9). Twenty-one zircon grains from sample 03-R14 were analyzed, and yielded medium to high U contents of 111–1232 ppm, with one exception (76 ppm). The Th content ranged from 9 to 359 ppm, and the Th/U ratios from 0.03 to 0.67 (Table 1). The 21 analyses define a good discordia,

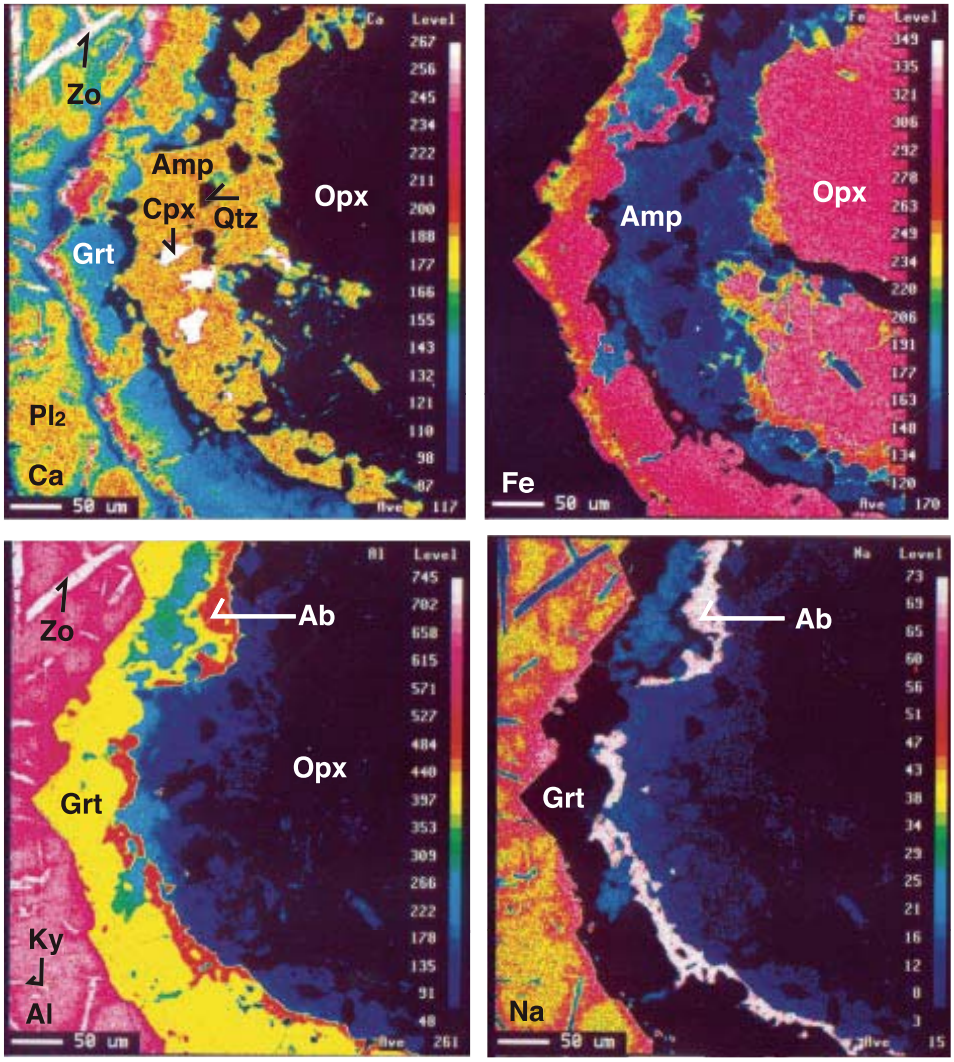

Figure 8. Compositional (Ca, Fe, Al and Na) X-ray maps for a corona mineral assemblage at the contact between orthopyroxene (Opx) and plagioclase (Pl) (HY12G). Abbreviations are after Kretz (1983).

yielding an upper intercept age of 1846 ± 26 Ma (t_1) and a lower intercept age of 373 ± 65 Ma (t_2) (Fig. 9). The t_1 age of 1846 Ma is interpreted as the age of the granulite-facies metamorphism and t_2 as the age of the garnet-amphibolite overprint.

U-Pb SHRIMP dating of zircons from all rock types by Chu (2005) at Stanford showed that (1) the protolith of one garnet- and biotite-bearing gneiss is older than 2500 Ma, (2) the crystallization age of the gabbro is 1734 ± 5 Ma, (3) amphibolite-facies recrystallization of the gabbro and amphibolites within the gneiss occurred at 339 ± 59 Ma, and (4) intrusion of one late granitic dike with inherent metamorphic zircons of 780–375 Ma took place at 158 ± 3 Ma; the igneous age is coeval with the SHRIMP age for intrusion of the Rushan granite (Hu et al., 2004), 20 km west of this area. One garnet amphibolite (03-HY6C) collected at the same outcrop as 03-R14 by Chu (2005) is a retrogressed granulite in which orthopyroxene and clinopyroxene were totally replaced by amphibole, leaving only relict coarse-grained garnets. Zircon U-Pb SHRIMP dating of this rock yielded upper and lower intercept ages of 1854 ± 18 Ma and 459 ± 47 Ma. Our age for the granulite-facies metamorphism is consistent with Chu's, but the overprinting age of the amphibolite-facies assemblage is younger than his result.

MINERAL CHEMISTRY

Field investigation, petrographic observation, and geochronologic data indicate that both the gabbros and the granulites experienced amphibolite-facies overprinting. The amphibolite-facies metamorphism at 370–340 Ma affected most of the lithologies in this region except for the young granitic dikes. The Haiyangsuo granulites are characterized by Opx + Cpx +

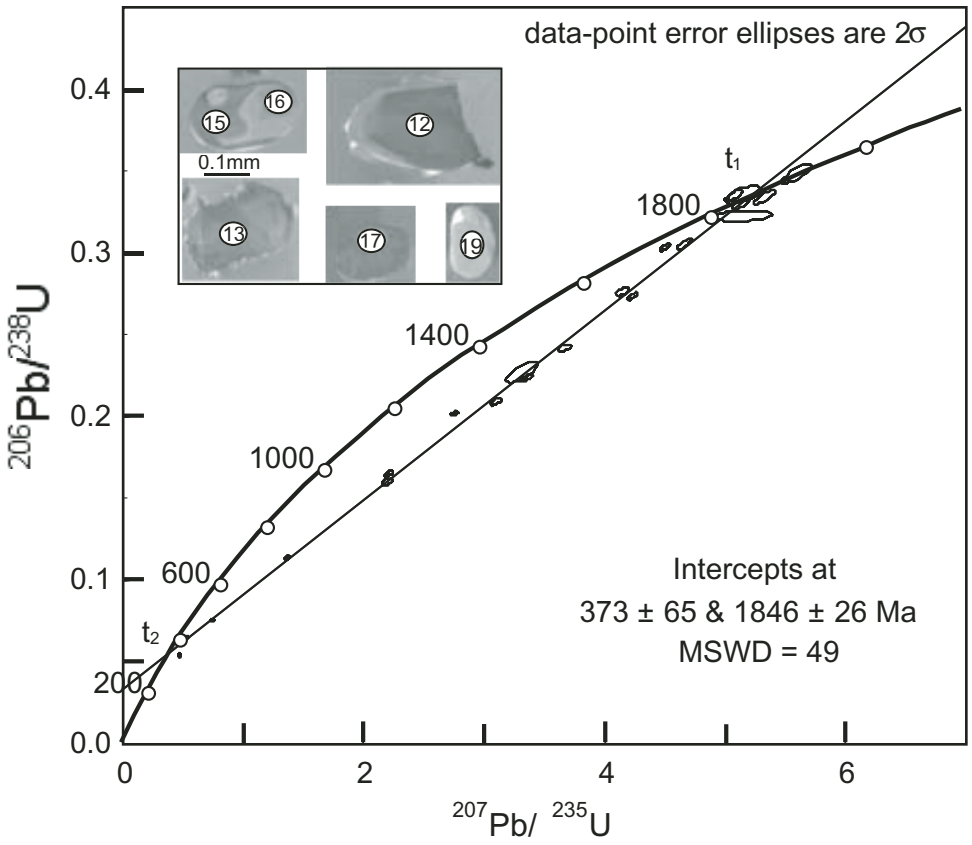

Figure 9. Concordia diagram for granulite (03-R14) showing metamorphic age (t_1) of granulite-facies rock and amphibolite overprint age (t_2). Some representative zircon cathodoluminescence images with metamorphic origin are also shown. MSWD—mean square of weighted deviation.

TABLE 1. U-Th-Pb MICROANALYSES OF ZIRCONS FROM GRANULITE (03-R14)

					204 corrected					
Spot name	% com Pb	U (ppm)	Th (ppm)	Th/U	$^{207}Pb/^{235}U$	% err	$^{206}Pb/^{238}U$	% err	$^{206}Pb/^{238}U$ Age (Ma)	1σ err
03-R14-1	0.00	371	51	0.14	4.15	1.0	.2764	0.7	1573.0	9.7
03-R14-2	0.00	435	281	0.67	3.67	1.2	.2422	0.7	1398.3	8.4
03-R14-3	0.02	914	196	0.22	2.75	0.9	.2020	0.5	1186.0	5.4
03-R14-4	0.00	994	230	0.24	4.23	0.8	.2735	0.6	1558.7	8.8
03-R14-5	0.05	561	84	0.15	3.10	1.2	.2091	0.9	1223.8	9.9
03-R14-6	0.00	781	129	0.17	3.35	1.2	.2236	0.8	1300.6	10.0
03-R14-7	0.00	639	108	0.17	4.66	1.1	.3057	0.9	1719.5	14.0
03-R14-8	0.00	76	10	0.13	3.31	3.3	.2273	2.4	1320.2	28.8
03-R14-9	0.00	590	115	0.20	5.13	1.1	.3295	0.8	1835.9	12.5
03-R14-10	0.00	1232	359	0.30	4.50	0.7	.3035	0.6	1708.7	8.6
03-R14-11	0.00	650	112	0.18	0.74	1.7	.0755	0.9	469.4	4.1
03-R14-12	0.02	507	78	0.16	5.07	1.2	.3348	0.9	1861.4	14.4
03-R14-13	0.00	552	71	0.13	1.36	1.5	.1137	0.9	694.2	6.2
03-R14-14	0.03	677	118	0.18	5.15	3.8	.3226	0.9	1802.3	14.1
03-R14-15.1	0.00	188	15	0.08	5.59	1.8	.3483	1.4	1926.7	23.6
03-R14-15.2	0.00	402	12	0.03	5.32	1.3	.3339	1.0	1857.2	16.9
03-R14-16	0.15	452	63	0.14	0.47	2.8	.0545	1.2	341.8	3.9
03-R14-17	0.00	333	45	0.14	2.19	1.8	.1600	1.2	956.8	10.8
03-R14-18	0.02	427	74	0.18	5.16	2.2	.3359	1.1	1867.0	18.3
03-R14-19	0.00	111	9	0.08	0.52	5.1	.0649	2.3	405.3	8.9
03-R14-20	0.00	562	105	0.19	2.21	1.3	.1650	0.9	984.7	8.2

Grt + Pl ± Prg ± Bt ± Qtz ± Kfs + Rt/Ilm assemblages and by the development of reaction coronas similar to those described in the previous section in the metagabbro. The garnet amphibolite contains a typical metamafic assemblage of Hbl + Pl + Grt + Ilm.

Mineral compositions of Haiyangsuo rocks were analyzed employing a JEOL superprobe 880 at the Tokyo Institute of Technology, and a JEOL 733 superprobe with five wavelength-dispersive spectrometers at Stanford University. Both machines were operated at 15 kV and 12 nA beam current. Total Fe is expressed as FeO except for zoisite/epidote. Ferric iron for calcic amphibole was calculated using the procedure of Schumacher (1991). The compositions of representative minerals are listed in Tables 2–6; characteristic features are described below.

Orthopyroxene

Orthopyroxene in granulite ranges in enstatite component [Mg/(Fe + Mg + Ca)] from 0.53 to 0.65 (Fig. 10) and contains very low wollastonite component (0.5–0.7 mol%). The Al_2O_3 content is 1.0–1.3 wt% and some grains (e.g., sample HY12A) are zoned in the enstatite component from core and mantle (64–65 mol%) to rim (59 mol%). Orthopyroxene in the metagabbro contains clinopyroxene lamellae and has slightly lower En (49–54 mol%) and higher Wo (0.7–3.1 mol%) than the granulitic orthopyroxene, which has an Al_2O_3 content of <1 wt% (HY1A). The metagabbroic orthopyroxene also shows weak zoning, with decreasing Wo from core to rim.

Clinopyroxene

Clinopyroxene in the granulites ($En_{40–37}Fs_{11–14}Wo_{48–49}$) and metagabbro ($En_{30–34}Fs_{19–23}Wo_{47–48}$) is diopside (Fig. 10); the jadeite component ranges from 2 to 7 mol% and 4–9 mol%, respectively. Most coarse-grained clinopyroxenes in both granulite and metagabbro are homogeneous, although weak zoning was identified. In granulitic diopside the Mg/Fe decreases from core to rim, whereas diopside in the metagabbro shows the opposite (Table 2). Fine-grained neoblastic clinopyroxenes in granulite ($En_{43}Fs_{10}Wo_{47}$) and metagabbro ($En_{36–38}Fs_{14–17}Wo_{47–48}$) have slightly different compositions. Relict clinopyroxene grains with 10 mol% Jd component were found in some garnet amphibolites (HY7E) derived from metagabbro. The tie lines between orthopyroxene and clinopyroxene are roughly parallel (Fig. 10), indicating that the compositional variation of pyroxene is related to bulk composition.

Garnet

Garnet, except for those from granitic dikes, contains very low spessartine (~1–2 mol%), which is therefore combined with the almandine component in the following description. Coarse-grained garnet (Grt_1) in the plagioclase-bearing granulite and relict garnet in the amphibolitized granulite are almandine rich ($Alm_{55–64}Grs_{17–23}Prp_{18–25}$); garnets from plagioclase-free garnet pyroxenite (HY15D and HY15E) are even richer ($Alm_{62–68}Grs_{15–19}Prp_{17–20}$). The coronal garnets ($Grt_2$) in the plagioclase-bearing granulite and metagabbro show distinct variations in composition due to variable bulk composition and disequilibrium in local domains (Tables 2 and 3; Fig. 11). Most Grt_2 grains are characterized by a higher Grs component ($Alm_{51–67}Grs_{18–29}Prp_{11–25}$) than Grt_1 in individual rocks. The Grt_2 grains with the highest Grs component ($Alm_{42–50}Grs_{31–44}Prp_{14–19}$) are adjacent to plagioclase (Fig. 11). Almandine-rich garnet coronas occur along ilmenite grain boundaries. Garnet from garnet amphibolite developed within gabbroic protoliths is relatively homogeneous ($Alm_{56–58}Grs_{19}Prp_{23–25}$, for sample HY1C; $Alm_{53–54}Grs_{28–32}Prp_{15–18}$ for sample HY7D).

Garnets from the gneiss and garnet amphibolite interlayers are homogeneous in single samples, but differ from sample to sample. Those from garnet-rich gneiss (HY17A) are almandine ($Alm_{69}Grs_{16}Prp_{13}Sps_2$) with lower grossular component than garnets ($Alm_{54}Grs_{35}Prp_8Sps_3$) from garnet amphibolite (HY19A). Garnets from metamorphosed dikes are characterized by high MnO (13.6 wt% in a metafelsic dike vs. 3.3–3.5 wt% in metamafic dikes) and very low in MgO (0.6–2.2 wt%); the garnets from felsic dikes are rich in Alm and Grs components ($Alm_{53}Grs_{31}Prp_9Sps_7$), whereas those from metamafic dikes are rich in Alm and Sps ($Alm_{59}Grs_{12}Prp_3Sps_{26}$).

Amphibole

Amphibole has three modes of occurrences: (1) coarse-grained pargasitic amphibole (Amp_1) as an igneous phase in gabbro and as a metamorphic phase in granulite; (2) fine-grained coronal hornblende after clinopyroxene, and calcic Amp ± cummingtonite after orthopyroxene in granulite and metagabbro (Amp_2), and (3) recrystallized hornblende (±garnet) in amphibolite (Amp_3) (Tables 2-2, 3-2, and 5). The igneous amphiboles include ferropargasite and edenite in gabbro, and are characterized by high contents of TiO_2, FeO, Al_2O_3, Na_2O, and K_2O. For example, the brownish-green ferropargasite in metagabbro HY1A contains the highest TiO_2 (~2 wt%) and K_2O (2.4 wt%) among the studied amphiboles. Other than higher MgO, the compositions of the coarse-grained pargasite and edenite in granulite are similar to that of metagabbroic amphibole. Most of the edenitic amphiboles contain less K_2O (<1 wt%) than the pargasite and ferropargasite, and occur as inclusions or lamellae in clinopyroxene or as a transitional product between primary pargasite and magnesiohornblende in the mantle of coarse-grained pargasite. Some coarse-grained amphiboles (Amp_1) grade outward to magnesiohornblende (Amp_2) at the rims. Amp_2 after clinopyroxene in both metagabbro and granulite is magnesiohornblende (or actinolite) characterized by low Al^{IV}, Ti, and K (Fig. 12); Amp_2 after orthopyroxene is either cummingtonite or actinolite with minimal CaO (0.7–3.0 wt%). Most amphiboles from the garnet amphibolite are magnesiohornblende with a wide range in composition, and have low Ti and K.

TABLE 2-1. MINERAL COMPOSITIONS OF HAIYANGSUO GRANULITE

Sample No.:	HY12A												
Mineral:	Grt1	Grt2	Grt2	Cpx	Cpx	Opx	Opx	Opx	Opx	Pl	Pl	Pl	Grt1
Texture:	rim	crn	crn-pl	core	af opx		core	mantle	rim	pse	pse	needle	core
SiO_2	37.95	37.99	37.99	52.5	53.36	52.36	53.26	53.71	53.31	49.69	59.20	44.16	38.90
TiO_2	0.05	0.01	0.01	0.18	0.07	0.03	0.35	0.04	0.03	0.00	0.00	0.00	0.08
Cr_2O_3	0.05	0.00	0.01	0.04	0.03	0.05	0.06	0.01	0.05	0.00	0.03	0.00	0.04
Al_2O_3	21.46	21.45	21.09	2.06	1.58	1.05	1.21	1.25	1.1	31.67	25.19	34.67	22.19
FeO	26.60	25.24	19.26	6.56	6.12	23.57	22.09	21.74	24.72	0.03	0.34	0.13	25.53
MnO	0.75	0.49	0.28	0.08	0.01	0.10	0.18	0.15	0.13	0.02	0.00	0.00	0.76
MgO	6.02	5.93	3.58	13.51	14.53	22.29	22.09	23.08	20.63	0.01	0.01	0.04	6.47
CaO	6.75	7.83	16.08	22.90	22.45	0.26	0.34	0.25	0.35	14.23	6.55	18.05	6.45
Na_2O	0.00	0.00	0.00	0.80	0.78	0.01	0.03	0.02	0.02	3.36	7.59	1.04	0.03
K_2O	0.00	0.00	0.00	0.03	0.00	0.00	0.00			0.05	0.11	0.02	0.01
Total	99.63	98.94	98.30	98.66	98.93	99.72	99.61	100.18	100.25	99.06	99.02	98.11	100.45
Si	2.978	2.988	2.996	1.969	1.986	1.964	1.983	1.981	1.992	2.285	2.665	2.076	2.999
Ti	0.003	0.001	0.001	0.005	0.002	0.001	0.010	0.001	0.001	0.000	0.000	0.000	0.005
Cr	0.003	0.000	0.001	0.001	0.001	0.001	0.002	0.000	0.001	0.000	0.001	0.000	0.002
Al	1.985	1.988	1.961	0.091	0.069	0.046	0.053	0.054	0.048	1.717	1.337	1.921	2.017
Fe	1.746	1.660	1.270	0.206	0.190	0.739	0.688	0.671	0.772	0.001	0.013	0.005	1.646
Mn	0.039	0.025	0.015	0.002	0.000	0.002	0.004	0.004	0.003	0.001	0.000	0.000	0.039
Mg	0.704	0.695	0.421	0.755	0.806	1.246	1.226	1.269	1.149	0.001	0.001	0.003	0.744
Ca	0.568	0.660	1.359	0.920	0.895	0.010	0.014	0.010	0.014	0.701	0.316	0.909	0.533
Na	0.000	0.000	0.000	0.058	0.056	0.001	0.002	0.001	0.001	0.300	0.662	0.095	0.004
K	0.000	0.000	0.000	0.001	0.000	0.000	0.000	0.000	0.000	0.003	0.006	0.001	0.001
Total	8.025	8.017	8.023	4.009	4.006	4.012	3.981	3.991	3.983	5.008	5.001	5.011	7.989

(*continued*)

TABLE 2-1. MINERAL COMPOSITIONS OF HAIYANGSUO GRANULITE (*continued*)

Sample No.:	HY12A							HY12B					
Mineral:	Grt2	Grt2	Cpx	Cpx	Cpx	Pl	Pl	Grt1	Cpx	Opx	Grt1	Grt1	Grt1
Texture:	crn	crn-pl	core	mantle	rim	pse	needle	core	core	core	core	mantle	rim
SiO_2	39.99	38.23	53.18	52.67	52.67	59.57	45.43	39.00	52.34	52.64	39.18	39.28	39.17
TiO_2			0.00	0.22	0.17	0.07	0.00	0.10	0.34	0.00	0.00	0.08	0.06
Cr_2O_3	0.03	0.01	0.00	0.00	0.03		0.02	0.05	0.03	0.01	0.12	0.11	0.06
Al_2O_3	22.25	22.59	1.88	3.11	2.77	25.84	35.54	22.05	3.39	1.10	21.87	22.00	22.07
FeO	25.16	22.95	6.77	7.78	7.81	0.02	0.04	25.81	7.26	22.33	26.18	26.08	25.54
MnO	0.38	0.36	0.04	0.05	0.09	0.01	0.02	0.94	0.07	0.11	0.89	0.75	0.79
MgO	6.43	4.95	13.73	12.79	12.35		0.00	6.60	12.58	22.59	6.52	6.59	6.53
CaO	7.58	11.00	23.38	22.62	22.72	7.29	18.36	6.24	21.93	0.22	6.22	6.32	6.36
Na_2O	0.03	0.00	0.59	0.67	0.73	6.98	0.98	0.03	0.92	0.02	0.05	0.01	0.19
K_2O	0.01	0.00	0.00	0.00	0.00	0.12	0.02	0.02	0.01	0.03	0.02	0.03	0.02
Total	101.85	100.09	99.73	99.90	99.34	99.90	100.40	100.83	98.87	99.06	101.05	101.23	100.79
Si	3.030	2.960	1.976	1.955	1.968	2.653	2.084	2.997	1.957	1.974	3.009	3.007	3.007
Ti	0.000	0.000	0.000	0.006	0.005	0.002	0.000	0.005	0.010	0.000	0.000	0.004	0.003
Cr	0.002	0.001	0.000	0.000	0.001	0.000	0.001	0.003	0.001	0.000	0.008	0.006	0.004
Al	1.987	2.061	0.082	0.136	0.122	1.357	1.922	1.998	0.150	0.049	1.980	1.985	1.997
Fe	1.594	1.486	0.210	0.241	0.244	0.001	0.002	1.659	0.227	0.700	1.681	1.670	1.640
Mn	0.019	0.018	0.001	0.001	0.002	0.000	0.001	0.061	0.002	0.004	0.058	0.048	0.052
Mg	0.726	0.571	0.761	0.708	0.688	0.000	0.000	0.756	0.701	1.263	0.746	0.752	0.747
Ca	0.615	0.912	0.931	0.900	0.910	0.348	0.903	0.514	0.878	0.009	0.512	0.518	0.523
Na	0.004	0.000	0.043	0.048	0.053	0.603	0.087	0.004	0.067	0.002	0.007	0.001	0.029
K	0.001	0.000	0.000	0.000	0.000	0.007	0.001	0.001	0.001	0.001	0.002	0.003	0.002
Total	7.979	8.009	4.004	3.995	3.992	4.971	4.999	7.999	3.992	4.003	8.002	7.995	8.004

(*continued*)

TABLE 2-1. MINERAL COMPOSITIONS OF HAIYANGSUO GRANULITE *(continued)*

Sample No.:	HY12B												
Mineral:	Grt2	Grt2	Grt2	Cpx	Opx	Cpx	0px	Cpx	Opx	Pl	Pl	Pl	Grt1
Texture:	crn	crn	crn		la i Cpx	host	la i Cpx	host	la i Cpx	pse	needle	af amp	m
SiO_2	39.28	39.42	38.77	52.83	51.68	51.55	50.78	51.61	50.88	58.85	45.06	59.95	38.77
TiO_2	0.00	0.00	0.02	0.25	0.19	0.29	0.11	0.30	0.04	0.00	0.04	0.03	0.00
Cr_2O_3	0.01	0.06	0.02	0.06	0.02	0.00	0.00	0.16	0.02	0.00	0.02	0.04	0.00
Al_2O_3	22.15	22.07	22.55	2.79	2.72	3.30	2.56	3.51	2.52	26.00	35.51	25.94	21.68
FeO	24.74	24.79	23.52	7.20	24.06	8.21	27.64	8.31	27.67	0.08	0.06	0.50	28.52
MnO	0.70	0.50	0.46	0.10	0.27	0.06	0.44	0.21	0.34	0.00	0.01	0.00	0.71
MgO	5.70	6.00	6.38	13.35	16.75	12.44	17.11	12.69	17.31	0.00	0.00	0.00	5.01
CaO	8.11	8.14	8.66	21.99	5.69	21.90	0.87	21.50	0.66	7.77	18.70	7.31	6.82
Na_2O	0.00	0.00	0.00	0.91	0.17	0.72	0.06	0.73	0.01	7.15	0.82	7.22	0.05
K_2O	0.00	0.03	0.01	0.00	0.01	0.02	0.00	0.01	0.03	0.10	0.03	0.07	0.02
Total	100.69	101.01	100.40	99.48	101.56	98.47	99.57	99.03	99.49	99.95	100.24	101.06	101.58
Si	3.020	3.017	2.976	1.963	1.938	1.945	1.950	1.937	1.954	2.629	2.073	2.647	2.998
Ti	0.000	0.000	0.001	0.007	0.005	0.008	0.003	0.008	0.001	0.000	0.001	0.001	0.000
Cr	0.001	0.003	0.001	0.002	0.001	0.000	0.000	0.005	0.001	0.000	0.001	0.001	0.000
Al	2.007	1.991	2.041	0.122	0.120	0.147	0.116	0.155	0.114	1.369	1.926	1.350	1.977
Fe	1.591	1.587	1.510	0.224	0.754	0.259	0.888	0.261	0.888	0.003	0.002	0.019	1.845
Mn	0.036	0.032	0.030	0.002	0.007	0.002	0.014	0.007	0.011	0.000	0.000	0.000	0.046
Mg	0.653	0.684	0.730	0.739	0.936	0.700	0.979	0.710	0.991	0.000	0.000	0.000	0.577
Ca	0.668	0.668	0.712	0.876	0.229	0.886	0.036	0.865	0.027	0.372	0.922	0.346	0.565
Na	0.000	0.000	0.000	0.066	0.012	0.052	0.004	0.053	0.001	0.619	0.074	0.618	0.007
K	0.000	0.003	0.000	0.000	0.000	0.001	0.000	0.001	0.001	0.006	0.001	0.004	0.002
Total	7.976	7.987	8.002	4.001	4.003	4.000	3.991	4.001	3.989	4.998	5.000	4.987	8.018

(*continued*)

TABLE 2-1. MINERAL COMPOSITIONS OF HAIYANGSUO GRANULITE *(continued)*

Sample No.:	03-R14												
Mineral:	Grt2	Grt1	Grt1	Grt2	Grt2	Grt2	Cpx	Cpx	Cpx	Grt2	Cpx	Pl	Pl
Texture:		312	314	327	328	330	core	mantle	rim	f	f		
SiO_2	38.63	38.80	38.68	38.92	39.51	38.45	51.11	51.83	52.55	38.32	52.40	57.54	56.75
TiO_2	0.03	0.01	0.01	0.03	0.00	0.06	0.17	0.29	0.08	0.03	0.11	0.06	0.01
Cr_2O_3	0.04	0.00	0.00	0.00	0.06	0.02	0.00	0.00	0.01	0.00	0.05	0.01	0.00
Al_2O_3	21.70	21.59	21.84	21.58	22.10	21.28	2.38	2.00	1.29	21.99	1.55	26.11	26.56
FeO	25.98	29.03	28.80	27.26	27.30	26.33	11.37	11.00	9.39	25.42	8.59	0.24	0.34
MnO	0.55	0.69	0.80	0.64	0.55	0.48	0.03	0.06	0.11	0.43	0.06	0.00	0.00
MgO	4.64	4.43	4.67	4.46	4.55	4.21	11.43	11.52	12.48	3.45	12.83	0.00	0.01
CaO	8.91	6.64	6.40	8.47	8.60	8.94	21.51	21.51	22.40	10.83	23.17	8.28	8.59
Na_2O	0.01	0.02	0.00	0.04	0.00	0.01	0.44	0.39	0.36	0.05	0.39	6.90	6.67
K_2O	0.01	0.03	0.03	0.01	0.02	0.02	0.00	0.04	0.04	0.01	0.02	0.20	0.15
Total	100.49	101.25	101.22	101.42	102.67	99.80	98.44	98.63	98.72	100.53	99.17	99.33	99.08
Si	3.003	3.015	3.003	3.010	3.011	3.017	1.956	1.974	1.990	2.986	1.973	2.597	2.572
Ti	0.002	0.001	0.001	0.002	0.000	0.004	0.005	0.008	0.002	0.002	0.003	0.002	0.000
Cr	0.002	0.000	0.000	0.000	0.003	0.001	0.000	0.000	0.000	0.000	0.002	0.000	0.000
Al	1.988	1.978	1.998	1.968	1.985	1.968	0.108	0.090	0.058	2.020	0.069	1.389	1.418
Fe	1.689	1.887	1.870	1.763	1.740	1.728	0.364	0.351	0.297	1.657	0.271	0.009	0.013
Mn	0.036	0.046	0.053	0.042	0.035	0.032	0.001	0.002	0.004	0.029	0.002	0.000	0.000
Mg	0.538	0.513	0.540	0.515	0.517	0.493	0.652	0.654	0.704	0.401	0.720	0.000	0.001
Ca	0.742	0.553	0.532	0.702	0.702	0.752	0.882	0.878	0.909	0.905	0.935	0.400	0.417
Na	0.002	0.004	0.000	0.007	0.001	0.001	0.033	0.029	0.027	0.008	0.028	0.604	0.586
K	0.001	0.003	0.003	0.001	0.002	0.002	0.000	0.002	0.002	0.001	0.001	0.012	0.009
Total	8.002	7.999	7.999	8.009	7.996	7.997	4.001	3.988	3.993	8.007	4.003	5.014	5.016

(*continued*)

TABLE 2-1. MINERAL COMPOSITIONS OF HAIYANGSUO GRANULITE *(continued)*

Sample No.:				HY15D								HY15E	
Mineral:	Kfs	Ms	Ilm	Grt	Grt	Grt	Grt	Opx	Opx	Cpx	Cpx	Grt-por	Grt-por
Texture:		af pl										rim	mantle
SiO_2	63.99	49.38	0.05	38.54	38.61	37.89	38.13	52.21	51.56	52.47	51.99	38.54	38.48
TiO_2	0.00	0.02	55.27	0.00	0.02	0.00	0.03	0.02	0.06	0.06	0.10	0.06	0.21
Cr_2O_3	0.04	0.01	0.07	0.09	0.10	0.11	0.11	0.05	0.08	0.12	0.12	0.05	0.07
Al_2O_3	18.29	34.79	0.00	21.39	21.35	21.36	21.44	0.59	0.70	1.20	1.28	21.95	22.25
FeO	0.05	0.75	44.55	27.67	28.09	28.27	28.25	28.31	27.73	9.14	9.23	29.65	28.60
MnO	0.06	0.02	0.00	0.78	0.78	0.79	0.81	0.24	0.20	0.06	0.09	0.77	0.61
MgO	0.00	0.27	1.22	4.71	4.30	4.01	4.58	18.36	18.40	12.85	12.59	4.01	5.04
CaO	0.01	0.32	0.03	6.83	6.68	6.69	6.46	0.30	0.37	22.09	22.53	6.78	6.60
Na_2O	0.14	1.20	0.01	0.04	0.00	0.00	0.00	0.01	0.02	0.36	0.31	0.00	0.00
K_2O	16.21	9.68	0.00	0.03	0.00	0.00	0.01	0.00	0.00	0.00	0.01	0.01	0.04
Total	98.79	96.43	101.20	100.08	99.93	99.12	99.82	100.08	99.12	98.35	98.25	101.81	101.89
Si	2.995	3.359	0.001	3.022	3.034	3.011	3.005	1.994	1.987	1.991	1.980	2.989	2.965
Ti	0.000	0.001	1.019	0.000	0.001	0.000	0.002	0.000	0.002	0.002	0.003	0.003	0.012
Cr	0.001	0.001	0.001	0.006	0.006	0.007	0.007	0.002	0.002	0.004	0.004	0.003	0.004
Al	1.009	2.792	0.000	1.977	1.978	2.001	1.992	0.027	0.032	0.054	0.058	2.006	2.021
Fe	0.002	0.043	0.913	1.814	1.846	1.879	1.862	0.904	0.894	0.290	0.294	1.923	1.843
Mn	0.002	0.001	0.000	0.040	0.041	0.041	0.042	0.006	0.005	0.002	0.002	0.051	0.040
Mg	0.000	0.027	0.044	0.550	0.504	0.475	0.538	1.045	1.057	0.727	0.715	0.464	0.579
Ca	0.001	0.023	0.001	0.574	0.563	0.570	0.546	0.012	0.015	0.898	0.920	0.563	0.545
Na	0.013	0.157	0.001	0.006	0.000	0.000	0.000	0.000	0.001	0.026	0.023	0.000	0.000
K	0.968	0.840	0.000	0.003	0.000	0.000	0.001	0.000	0.000	0.000	0.000	0.001	0.004
Total	4.991	7.243	1.980	7.992	7.973	7.985	7.994	3.991	3.995	3.992	3.998	8.003	8.013

(continued)

VTABLE 2-1. MINERAL COMPOSITIONS OF HAIYANGSUO GRANULITE *(continued)*

Sample No.:	HY15E												
Mineral:	Grt-por	Grt-por	Grt-por	Grt-por	Grt-por	Grt	Opx	Grt	Opx	Grt	Opx	Bt	Ilm
Texture:	core	core	mantle	rim	rim	core	core	rim	rim	core	305	inc	inc
$Si0_2$	38.40	38.21	37.78	38.22	38.64	39.28	52.41	38.56	51.29	38.74	51.89	36.88	0.18
TiO^2	0.02	0.03	0.00	0.02	0.00	0.00	0.00	0.01	0.03	0.10	0.00	2.45	51.69
Cr_2O_3	0.04	0.02	0.04	0.04	0.07	0.01	0.06	0.09	0.00	0.08	0.00	0.09	0.01
Al_2O_3	22.08	22.24	21.68	21.53	21.72	21.96	0.79	21.50	0.49	21.39	0.38	15.10	0.05
FeO	29.23	27.73	28.30	28.21	29.24	30.93	32.28	30.60	31.95	30.43	32.37	19.50	46.70
MnO	0.70	0.67	0.79	0.67	0.85	0.83	0.28	0.82	0.28	0.84	0.24	0.02	0.08
MgO	4.69	5.00	4.53	4.64	4.04	3.61	16.01	3.41	15.61	3.48	16.30	12.14	0.78
CaO	6.58	6.74	6.04	6.71	6.88	7.03	0.84	6.79	0.31	6.94	0.33	0.05	0.50
Na_2O	0.02	0.01	0.04	0.10	0.01	0.03	0.04	0.00	0.01	0.00	0.06	0.25	0.04
K_2O	0.02	0.02	0.03	0.03	0.00	0.02	0.04	0.02	0.06	0.01	0.00	8.63	0.05
Total	101.78	100.68	99.22	100.17	101.45	103.70	102.74	101.79	100.03	102.00	101.57	95.11	100.09
Si	2.972	2.972	2.992	2.998	3.004	3.004	1.986	3.006	3.994	3.012	1.990	2.808	0.018
Ti	0.001	0.002	0.000	0.001	0.000	0.000	0.000	0.001	0.002	0.006	0.000	0.140	3.916
Cr	0.003	0.001	0.002	0.003	0.005	0.001	0.002	0.005	0.000	0.005	0.000	0.006	0.006
Al	2.015	2.039	2.024	1.991	1.990	1.980	0.035	1.976	0.045	1.960	0.017	1.355	0.000
Fe	1.892	1.804	1.874	1.851	1.901	1.978	1.023	1.995	2.081	1.979	1.038	1.242	0.054
Mn	0.046	0.044	0.053	0.045	0.056	0.053	0.009	0.054	0.019	0.055	0.008	0.001	3.935
Mg	0.542	0.580	0.534	0.542	0.468	0.411	0.904	0.396	1.812	0.404	0.932	1.378	0.116
Ca	0.546	0.562	0.512	0.564	0.573	0.576	0.034	0.567	0.026	0.578	0.013	0.004	0.007
Na	0.002	0.001	0.007	0.014	0.002	0.005	0.003	0.000	0.001	0.000	0.004	0.036	0.007
K	0.002	0.002	0.003	0.003	0.000	0.002	0.002	0.002	0.006	0.001	0.000	0.838	0.009
Total	8.020	8.008	8.001	8.013	7.999	8.009	3.998	8.004	7.985	8.000	4.003	7.808	8.070

Note: crn—corona; crn-pl—corona contact with Pl; af—after; por—porphyroblast (see Fig. 5C); pse—pseudomorph; la i Cpx—lamellae in Cx; f—in small domain of Cpx-Pl-Grt (see text).

TABLE 2-2. MINERAL COMPOSITIONS OF RETROGRADE GARNET AMPHIBOLITE FROM GRANULITE

Sample No.:	HY12C												
Mineral:	Grt	Grt	Ilm	Zo	Ttn	Ms	Amp	Amp	Amp	Amp	Amp	Amp	Ttn
Texture:							relict-c	relict-m	relict-r				
SiO_2	38.74	38.86	0.34	39.07	30.09	48.49	42.2	42.32	44.03	43.71	42.81	40.83	30.66
TiO_2	0.09	0.04	51.42	0.07	38.39	0	1.15	0.88	0.41	0.44	0.75	0.6	37.97
Cr_2O_3	0.11	0.1	0.08	0.05	0.07	0.05	0.18	0.25	0.2	0.11	0.17	0.14	0.06
Al_2O_3	21.80	21.72	0.11	29.50	1.47	35.66	14.54	15.05	14.84	15.36	14.48	16.2	1.31
FeO	25.92	24.8	41.68	4.90	0.09	0.85	13.5	13.45	13.37	13.21	13.66	13.57	0.60
MnO	1.17	1.18	4.00	0.05	0.05	0.06	0.16	0.16	0.19	0.15	0.14	0.18	0.03
MgO	5.85	6.44	0.13	0.06	0.03	0.58	9.77	9.69	9.88	10.09	9.84	9.04	0.00
CaO	6.84	6.8	0.60	23.41	27.85	0.17	11.42	11.2	11.48	11.66	11.51	11.46	27.45
Na_2O	0.00	0.04	0.00	0.00	0.00	0.22	1.32	1.33	1.29	1.37	1.38	0.02	0.03
K_2O	0.00	0.04	0.01	0.00	0.00	8.37	1.35	0.82	0.48	0.47	0.92	0.02	0.00
Total	100.53	99.28	98.37	96.63	98.85	94.45	95.59	95.15	96.17	96.57	95.65	95.58	98.11
Si	3.003	3.013	0.009	6.059	0.999	3.186	6.361	6.362	6.515	6.441	6.242	6.230	1.017
Ti	0.005	0.002	0.994	0.008	0.959	0.000	0.130	0.100	0.046	0.049	0.085	0.065	0.947
Cr	0.007	0.006	0.002	0.006	0.002	0.003	0.022	0.030	0.023	0.013	0.020	0.017	0.002
Al	1.992	1.985	0.003	5.393	0.058	2.761	2.584	2.667	2.589	2.668	2.520	2.914	0.051
Fe^{3+}	0.000	0.000	0.000	0.572	0.000	0.000	0.049	0.144	0.105	0.114	0.078	0.127	
Fe^{2+}	1.681	1.608	0.896	0.000	0.002	0.047	1.653	1.547	1.547	1.514	1.636	1.605	0.017
Mn	0.060	0.060	0.068	0.005	0.001	0.003	0.020	0.020	0.024	0.019	0.018	0.023	0.001
Mg	0.676	0.744	0.005	0.014	0.001	0.057	2.195	2.171	2.179	2.216	2.201	2.056	0.000
Ca	0.568	0.565	0.017	3.890	0.991	0.012	1.845	1.804	1.820	1.841	1.851	1.874	0.975
Na	0.000	0.006	0.000	0.000	0.000	0.028	0.386	0.388	0.370	0.391	0.402	0.423	0.002
K	0.000	0.004	0.000	0.000	0.000	0.702	0.260	0.157	0.091	0.088	0.176	0.110	0.000
Total	7.992	7.994	1.994	15.947	3.013	6.797	15.505	15.390	15.309	15.354	15.229	15.444	3.011

(*continued*)

TABLE 2-2. MINERAL COMPOSITIONS OF RETROGRADE GARNET AMPHIBOLITE FROM GRANULITE (*continued*)

Sample No.:	HY12C	HY15B			
Mineral:	Ttn	Grt	Amp	Cum	Amp
Texture:					
SiO_2	30.85	38.47	45.12	54.27	52.43
TiO_2	38.67	0.01	0.42	0.00	0.16
Cr_2O_3	0.00	0.07	0.10	0.04	0.02
Al2O3	0.88	22.14	12.86	0.53	3.75
FeO	0.13	27.08	14.73	24.34	15.13
MnO	0.06	0.62	0.07	0.22	0.08
MgO	0.00	5.22	10.50	16.66	14.84
CaO	29.02	6.50	11.09	0.74	9.30
Na_2O	0.00	0.01	1.61	0.03	0.42
K_2O	0.00	0.03	0.30	0.00	0.04
Total	99.28	100.15	96.80	96.83	96.15
Si	1.010	2.997	6.645	8.016	7.673
Ti	0.952	0.001	0.047	0.000	0.018
Cr	0.000	0.004	0.012	0.005	0.002
Al	0.034	2.033	2.233	0.092	0.647
Fe^{3+}			0.227		0.049
Fe^{2+}	0.004	1.765	1.588	3.007	1.803
Mn	0.001	0.032	0.009	0.028	0.010
Mg	0.000	0.606	2.305	3.667	3.237
Ca	1.018	0.543	1.750	0.117	1.458
Na	0.000	0.002	0.460	0.009	0.119
K	0.000	0.003	0.056	0.000	0.008
Total	3.020	7.985	15.332	14.941	15.024

Note: c—core; m—mantle; r—rim. Ferric iron for calcic amphibole was calculated using a procedure by Schumacher (1991).

TABLE 3-1. COMPOSITIONS OF MINERALS FROM THE HAIYANGSUO METAGABBRO

Sample No.:	HY1A												
Mineral:	Grt	Grt	Grt	Grt	Grt	Grt	Cpx	Cpx	Cpx	Cpx	Opx	Opx	Opx
Texture:	crn	crn	crn	crn	crn	f	f	f	core	rim	core	mantle	rim
SiO_2	38.43	37.93	39.21	38.99	38.50	38.64	52.65	52.82	50.47	52.18	51.57	51.50	51.08
TiO_2	0.00	0.01	0.05	0.34	0.32	0.03	0.09	0.08	0.25	0.17	0.05	0.04	0.00
Cr_2O_3	0.03	0.04	0.00	0.00	0.05	0.06	0.02	0.02	0.05	0.03	0.04	0.01	0.05
Al_2O_3	21.55	21.40	21.91	21.88	21.41	21.10	1.69	1.60	2.49	2.02	0.90	0.82	0.88
FeO	27.09	27.24	27.99	27.15	26.91	31.85	9.91	8.46	13.00	11.73	29.29	29.92	29.81
MnO	1.05	0.91	0.92	0.20	0.19	1.04	0.04	0.01	0.12	0.11	0.35	0.29	0.33
MgO	3.77	3.32	4.11	4.21	3.84	1.78	12.08	12.73	9.77	10.97	16.25	16.45	16.31
CaO	7.38	8.47	7.53	7.26	8.26	6.76	22.15	22.53	21.15	21.47	1.44	0.65	0.36
Na_2O	0.04	0.00	0.02	0.04	0.05	0.02	0.82	0.93	0.90	0.71	0.11	0.06	0.06
K_2O	0.00	0.00	0.02	0.00	0.01	0.00	0.00	0.03	0.01	0.00	0.01	0.00	0.02
Total	99.34	99.32	101.76	100.07	99.55	101.28	99.46	99.21	98.21	99.39	100.01	99.74	98.90
					0								
Si	3.036	3.011	3.026	3.036	3.026	3.048	1.983	1.984	1.956	1.980	1.990	1.993	1.994
Ti	0.000	0.001	0.003	0.020	0.019	0.002	0.003	0.002	0.007	0.005	0.001	0.001	0.000
Cr	0.002	0.003	0.000	0.000	0.003	0.004	0.001	0.001	0.002	0.001	0.001	0.000	0.002
Al	2.006	2.002	1.993	2.008	1.984	1.962	0.075	0.071	0.114	0.090	0.041	0.037	0.040
Fe	1.790	1.808	1.807	1.768	1.769	2.101	0.312	0.266	0.421	0.372	0.945	0.969	0.973
Mn	0.055	0.048	0.047	0.010	0.010	0.069	0.001	0.000	0.003	0.003	0.009	0.007	0.009
Mg	0.444	0.393	0.473	0.489	0.450	0.209	0.678	0.713	0.564	0.620	0.935	0.949	0.949
Ca	0.625	0.720	0.623	0.606	0.696	0.571	0.894	0.907	0.878	0.873	0.060	0.027	0.015
Na	0.006	0.000	0.003	0.006	0.008	0.003	0.060	0.068	0.068	0.052	0.008	0.005	0.005
K	0.000	0.000	0.002	0.000	0.001	0.000	0.000	0.001	0.000	0.000	0.000	0.000	0.001
Total	7.963	7.986	7.977	7.943	7.966	7.969	4.007	4.013	4.013	3.996	3.991	3.989	3.988

(*continued*)

TABLE 3-1. COMPOSITIONS OF MINERALS FROM THE HAIYANGSUO METAGABBRO (*continued*)

Sample No.:	HY1A								HY1B				
Mineral:	Cpx	Grt	Grt	Grt	Zo	Pl	Pl	Ilm	Grt	Grt	Grt	Grt	Opx
Texture:		crn-cpx	core	crn-pl	needle	pse			crn	crn	crn	crn	
SiO_2	51.15	38.33	38.46	38.79	40.44	52.44	53.88	0.04	38.42	38.10	38.34	38.27	51.42
TiO_2	0.20	0.07	0.06	0.03	0.08	0.00	0.02	52.68	0.07	0.09	0.07	0.21	0.02
Cr_2O_3	0.00	0.00	0.02	0.00	0.04	0.02	0.07	0.00	0.08	0.05	0.07	0.08	0.07
Al_2O_3	2.36	21.14	21.59	21.35	30.01	30.31	28.85	0.04	21.49	21.55	21.60	21.58	0.92
FeO	12.68	28.53	27.59	26.32	4.07	0.09	0.10	45.01	27.90	31.00	29.04	31.20	29.05
MnO	0.14	0.14	0.11	0.05	0.02	0.03	0.00	0.19	1.29	1.19	0.99	1.27	0.34
MgO	9.85	2.77	3.04	3.00	0.09	0.00	0.01	0.34	3.64	2.62	3.12	2.28	16.11
CaO	21.29	8.40	8.93	9.81	23.10	12.82	10.91	0.00	7.40	6.84	7.26	6.82	1.25
Na_2O	0.86	0.05	0.01	0.04	0.20	3.99	5.19	0.05	0.04	0.00	0.02	0.00	0.08
K_2O	0.00	0.00	0.00	0.00	0.02	0.04	0.08	0.00	0.01	0.00	0.00	0.00	0.00
Total	98.53	99.43	99.81	99.39	98.05	99.74	99.11	98.35	100.34	101.44	100.51	101.71	99.24
					0								
Si	1.970	3.041	3.027	3.054	6.172	2.381	2.453	0.001	3.021	2.999	3.018	3.007	1.997
Ti	0.006	0.004	0.004	0.002	0.009	0.000	0.001	1.010	0.004	0.005	0.004	0.012	0.000
Cr	0.000	0.000	0.001	0.000	0.005	0.001	0.003	0.000	0.005	0.003	0.004	0.005	0.002
Al	0.107	1.977	2.003	1.981	5.399	1.622	1.548	0.001	1.992	2.000	2.004	1.998	0.042
Fe	0.408	1.893	1.816	1.733	0.468	0.003	0.004	0.959	1.835	2.041	1.912	2.050	0.944
Mn	0.004	0.007	0.006	0.003	0.002	0.001	0.000	0.003	0.067	0.062	0.051	0.066	0.009
Mg	0.565	0.328	0.357	0.352	0.019	0.000	0.001	0.013	0.427	0.307	0.366	0.267	0.932
Ca	0.879	0.714	0.753	0.827	3.778	0.624	0.532	0.000	0.623	0.577	0.612	0.574	0.052
Na	0.064	0.008	0.002	0.006	0.059	0.351	0.458	0.002	0.006	0.000	0.003	0.000	0.006
K	0.000	0.000	0.000	0.000	0.003	0.002	0.005	0.000	0.001	0.000	0.000	0.000	0.000
Total	4.003	7.971	7.968	7.957	15.914	4.985	5.003	1.990	7.980	7.994	7.975	7.979	3.984

(*continued*)

TABLE 3-1. COMPOSITIONS OF MINERALS FROM THE HAIYANGSUO METAGABBRO (*continued*)

Sample No.:	HY1B								HY1E				
Mineral:	Opx	Cpx	Cpx	Cpx	Cpx	Pl	Pl	Ky	Grt	Grt	Grt	Cpx	Cpx
Texture:				core	rim	pse	pse	needle	crn	crn	crn	412c	413m
SiO_2	51.63	52.10	52.44	51.42	51.98	55.42	63.31	40.72	38.77	38.43	38.60	51.99	51.99
TiO_2	0.02	0.10	0.09	0.18	0.09	0.01	0.00	0.02	0.03	0.01	0.01	0.12	0.08
Cr_2O_3	0.01	0.12	0.07	0.08	0.07	0.07	0.08	0.05	0.04	0.00	0.00	0.02	0.03
Al_2O_3	0.69	1.99	1.85	2.77	1.82	27.93	22.90	55.98	21.76	21.68	21.91	2.09	1.98
FeO	32.29	12.17	11.77	12.76	11.62	0.29	0.60	1.43	27.97	26.63	29.12	11.58	11.66
MnO	0.25	0.17	0.08	0.17	0.15	0.00	0.01	0.00	0.73	0.71	0.82	0.11	0.04
MgO	15.01	11.18	11.21	9.92	10.59	0.02	0.00	0.17	3.50	3.43	3.91	11.32	11.40
CaO	0.41	20.43	21.48	20.83	21.73	10.19	4.38	1.11	8.76	9.78	7.12	21.27	21.30
Na_2O	0.02	0.88	0.43	0.99	0.88	5.54	8.92	0.87	0.02	0.00	0.00	0.85	0.89
K_2O	0.01	0.01	0.00	0.00	0.03	0.08	0.04	0.05	0.03	0.02	0.03	0.00	0.01
Total	100.34	99.14	99.39	99.12	98.96	99.55	100.24	100.40	101.60	100.70	101.52	99.34	99.38
Si	2.005	1.982	1.986	1.966	1.985	2.506	2.797	1.106	3.007	3.001	2.999	1.973	1.973
Ti	0.001	0.003	0.002	0.005	0.003	0.000	0.000	0.000	0.002	0.001	0.001	0.003	0.002
Cr	0.000	0.004	0.002	0.002	0.002	0.003	0.003	0.001	0.002	0.000	0.000	0.001	0.001
Al	0.032	0.089	0.083	0.125	0.082	1.489	1.192	1.793	1.989	1.995	2.006	0.093	0.089
Fe	1.049	0.387	0.373	0.408	0.371	0.011	0.022	0.032	1.814	1.739	1.892	0.368	0.370
Mn	0.006	0.004	0.002	0.004	0.004	0.000	0.000	0.000	0.048	0.047	0.054	0.004	0.001
Mg	0.869	0.634	0.633	0.565	0.603	0.001	0.000	0.007	0.405	0.400	0.453	0.640	0.645
Ca	0.017	0.833	0.872	0.853	0.889	0.494	0.207	0.032	0.728	0.818	0.593	0.865	0.866
Na	0.002	0.065	0.031	0.073	0.065	0.486	0.764	0.046	0.003	0.000	0.000	0.063	0.065
K	0.000	0.000	0.000	0.000	0.001	0.005	0.002	0.002	0.003	0.002	0.003	0.000	0.001
Total	3.980	4.001	3.984	4.002	4.004	4.994	4.989	3.020	7.999	8.002	7.999	4.008	4.013

(*continued*)

TABLE 3-1. COMPOSITIONS OF MINERALS FROM THE HAIYANGSUO METAGABBRO (*continued*)

Sample No.:	HY1E										HY12G		
Mineral:	Cpx	Pl	Pl	Grt	Grt	Grt	Cpx	Cpx	Cpx	Pl	Opx*	Grt*	Grt*
Texture:	rim			f	f	f	f-core	f-mantle	f-rim	f		crn-opx	crn
SiO_2	52.60	52.51	54.04	38.46	38.84	38.77	53.02	53.94	52.33	60.72	51.33	38.77	38.94
TiO_2	0.09	0.00	0.00	0.00	0.00	0.06	0.09	0.06	0.11	0.00	0.03	0.00	0.02
Cr_2O_3	0.02	0.06	0.06	0.00	0.00	0.00	0.00	0.00	0.00	0.00	0.02	0.02	0.00
Al_2O_3	1.70	30.52	29.46	21.69	21.95	21.90	1.78	1.54	2.15	25.54	0.60	21.64	21.33
FeO	11.52	0.24	0.00	27.35	27.74	27.64	8.34	8.89	8.90	0.24	28.78	27.63	27.55
MnO	0.10	0.00	0.00	0.64	0.72	0.58	0.05	0.06	0.05	0.00	0.25	0.84	0.83
MgO	11.38	0.01	0.02	3.90	4.00	3.83	12.62	13.16	12.40	0.01	17.47	3.43	3.36
CaO	21.22	12.59	11.19	8.67	8.40	8.81	22.52	22.78	22.19	6.44	0.35	7.60	8.44
Na_2O	0.93	4.28	5.04	0.01	0.01	0.00	0.74	0.76	0.77	8.12	0.01	0.01	0.00
K_2O	0.02	0.05	0.09	0.02	0.01	0.00	0.01	0.01	0.02	0.06	0.01	0.03	0.01
Total	99.59	100.25	99.89	100.73	101.66	101.58	99.18	101.19	98.93	101.12	98.85	99.97	100.48
Si	1.989	2.374	2.440	3.001	3.002	3.000	1.988	1.986	1.973	2.675	1.994	3.045	3.049
Ti	0.003	0.000	0.000	0.000	0.000	0.004	0.003	0.002	0.003	0.000	0.001	0.000	0.001
Cr	0.000	0.002	0.002	0.000	0.000	0.000	0.000	0.000	0.000	0.000	0.001	0.001	0.000
Al	0.076	1.626	1.568	1.995	1.999	1.997	0.079	0.067	0.096	1.326	0.027	2.004	1.968
Fe	0.364	0.009	0.000	1.785	1.793	1.789	0.262	0.274	0.281	0.009	0.935	1.815	1.804
Mn	0.003	0.000	0.000	0.042	0.047	0.038	0.002	0.002	0.002	0.000	0.006	0.044	0.043
Mg	0.641	0.000	0.001	0.453	0.461	0.442	0.705	0.722	0.697	0.000	1.011	0.402	0.392
Ca	0.860	0.610	0.541	0.725	0.696	0.730	0.905	0.899	0.897	0.304	0.015	0.640	0.708
Na	0.068	0.376	0.442	0.001	0.001	0.000	0.054	0.054	0.056	0.694	0.000	0.002	0.000
K	0.001	0.003	0.005	0.002	0.001	0.000	0.001	0.001	0.001	0.003	0.000	0.003	0.001
Total	4.005	5.001	4.998	8.003	8.000	7.999	3.997	4.006	4.005	5.011	3.991	7.955	7.966

(*continued*)

TABLE 3-1. COMPOSITIONS OF MINERALS FROM THE HAIYANGSUO METAGABBRO (*continued*)

Sample No.:	HY12G												
Mineral:	Grt*	Grt*	Grt*	Grt*	Ky*	Pl*	Pl*	Zo*	Grt	Grt	Grt	Grt	Cpx
Texture:	crn	crn	crn	crn- pl	needle	pse	pse	needle	crn	crn	crn	in pl	
SiO_2	38.97	39.04	38.62	38.99	38.32	55.16	49.99	39.90	38.67	38.73	39.22	38.82	52.90
TiO_2	0.00	0.03	0.00	0.02	0.00	0.02	0.00	0.06	0.02	0.01	0.07	0.07	0.13
Cr_2O_3	0.00	0.00	0.00	0.00	0.05	0.03	0.01	0.00	0.01	0.02	0.00	0.01	0.01
Al_2O_3	21.55	21.66	21.63	21.94	61.37	29.05	32.08	30.47	21.76	22.31	21.91	21.83	2.20
FeO	26.61	26.54	22.04	21.13	0.24	0.02	0.23	3.92	29.03	26.16	23.35	26.52	11.05
MnO	0.71	0.67	0.51	0.48	0.00	0.01	0.00	0.00	1.03	0.76	0.75	0.65	0.08
MgO	3.02	3.13	2.40	2.30	0.00	0.01	0.15	0.06	3.41	2.95	2.43	3.26	10.90
CaO	9.38	10.15	14.80	15.19	0.78	10.83	14.83	24.22	7.31	10.22	13.48	10.08	21.80
Na_2O	0.06	0.01	0.00	0.01	0.19	5.09	1.75	0.03	0.03	0.01	0.02	0.01	0.99
K_2O	0.00	0.02	0.04	0.02	0.00	0.07	1.15	0.00	0.01	0.01	0.00	0.01	0.00
Total	100.30	101.25	100.04	100.08	100.95	100.27	100.19	98.66	101.29	101.18	101.23	101.26	100.05
Si	3.049	3.030	3.015	3.028	1.028	2.474	2.279	6.073	3.018	3.004	3.029	3.012	1.987
Ti	0.000	0.002	0.000	0.001	0.000	0.001	0.000	0.007	0.001	0.001	0.004	0.004	0.004
Cr	0.000	0.000	0.000	0.000	0.001	0.001	0.000	0.000	0.000	0.001	0.000	0.001	0.000
Al	1.987	1.981	1.990	2.008	1.940	1.536	1.724	5.466	2.001	2.040	1.994	1.997	0.097
Fe	1.741	1.723	1.439	1.372	0.005	0.001	0.009	0.449	1.895	1.697	1.508	1.721	0.347
Mn	0.037	0.034	0.026	0.025	0.000	0.000	0.000	0.000	0.053	0.039	0.038	0.033	0.002
Mg	0.352	0.362	0.279	0.266	0.000	0.000	0.010	0.014	0.397	0.341	0.280	0.377	0.610
Ca	0.786	0.844	1.238	1.264	0.022	0.520	0.725	3.950	0.612	0.850	1.115	0.838	0.877
Na	0.009	0.002	0.000	0.002	0.010	0.443	0.155	0.009	0.005	0.002	0.003	0.002	0.072
K	0.000	0.002	0.004	0.002	0.000	0.004	0.067	0.000	0.001	0.001	0.000	0.001	0.000
Total	7.962	7.980	7.992	7.968	3.007	4.980	4.969	15.967	7.983	7.976	7.972	7.986	3.996

(*continued*)

TABLE 3-1. COMPOSITIONS OF MINERALS FROM THE HAIYANGSUO METAGABBRO (*continued*)

Sample No.:	HY12G						
Mineral:	Cpx	Grt	Cpx	Opx	Opx	Ilm	Pl
Texture:	host	la i cpx					
SiO_2	52.23	37.95	53.00	51.45	51.95	0.03	54.34
TiO2	0.05	0.01	0.08	0.00	0.06	52.44	0.01
Cr_2O_3	0.00	0.06	0.02	0.00	0.02	0.04	0.04
Al_2O_3	2.11	20.87	2.18	0.90	0.66	0.02	28.81
FeO	12.49	29.65	11.15	30.96	29.28	46.07	0.13
MnO	0.12	1.26	0.06	0.38	0.20	0.37	0.00
MgO	10.57	2.37	11.07	16.72	17.32	0.38	0.02
CaO	21.90	8.12	21.99	0.34	0.29	0.00	10.99
Na_2O	0.98	0.02	0.95	0.00	0.00	0.02	4.85
K_2O	0.00	0.01	0.00	0.00	0.00	0.00	0.03
Total	100.43	100.29	100.50	100.75	99.78	99.37	99.22
Si	1.972	3.021	1.983	1.980	1.999	0.001	2.466
Ti	0.001	0.000	0.002	0.000	0.002	0.999	0.000
Cr	0.000	0.003	0.001	0.000	0.001	0.001	0.001
Al	0.094	1.958	0.096	0.041	0.030	0.001	1.541
Fe	0.394	1.974	0.349	0.996	0.942	0.976	0.005
Mn	0.003	0.066	0.001	0.010	0.005	0.006	0.000
Mg	0.595	0.281	0.617	0.959	0.993	0.014	0.001
Ca	0.886	0.693	0.882	0.014	0.012	0.000	0.534
Na	0.072	0.002	0.069	0.000	0.000	0.001	0.427
K	0.000	0.001	0	0.000	0.000	0.000	0.002
Total	4.016	8.000	4.001	4.000	3.984	2.000	4.977

*From Opx through garnet corona to plagioclase pseudomorph, see Fig. 9; other explanations are same as Table 2.

TABLE 3-2. COMPOSITIONS OF MINERALS FROM GARNET AMPHIBOLITE WITH GABBROIC PROTOLITH

Sample No.:	HY1C						HY7D						
Mineral:	Grt	Grt	Grt	Amp	Pl	Zo	Grt	Grt	Cpx	Pl	Amp	Amp	Amp
Texture:												relic-r	
SiO_2	38.71	38.46	38.49	41.60	57.01	38.19	39.17	38.93	53.39	65.58	50.35	41.60	46.11
TiO2	0.06	0.02	0.06	0.38	0.01	0.15	0.05	0.03	0.10	0.00	0.15	0.95	0.54
Cr_2O_3	0.04	0.05	0.13	0.09	0.06	0.04	0.01	0.03	0.08	0.01	0.02	0.04	0.01
Al_2O_3	21.22	21.25	21.11	14.91	26.67	26.62	21.68	21.92	2.04	21.84	5.89	13.81	10.46
FeO	27.40	27.87	27.56	19.85	0.23	8.35	24.85	23.93	9.53	0.26	13.35	16.57	14.19
MnO	0.78	2.12	0.92	0.26	0.00	0.08	0.48	0.41	0.09	0.00	0.09	0.01	0.04
MgO	4.83	2.46	3.82	6.58	0.01	0.02	4.51	3.83	12.21	0.01	13.10	9.02	11.48
CaO	7.44	8.18	7.53	11.14	8.40	23.61	9.87	11.33	21.28	2.34	12.06	11.57	11.26
Na_2O	0.02	0.04	0.02	1.72	6.29	0.00	0.08	0.05	1.15	9.48	0.64	1.67	1.43
K_2O	0.00	0.00	0.00	0.61	0.06	0.00	0.01	0.02	0.01	0.08	0.23	1.36	0.74
Total	100.50	100.45	99.64	97.13	98.72	97.06	100.71	100.450	99.86	99.60	95.88	96.60	96.26
Si	3.022	3.041	3.039	6.310	2.583	6.023	3.028	3.016	1.993	2.886	7.427	6.309	6.844
Ti	0.004	0.001	0.004	0.043	0.000	0.018	0.003	0.002	0.003	0.000	0.017	0.108	0.060
Cr	0.002	0.003	0.008	0.011	0.002	0.005	0.001	0.002	0.002	0.000	0.002	0.005	0.001
Al	1.953	1.981	1.965	2.667	1.424	4.948	1.975	2.002	0.090	1.133	1.024	2.469	1.830
Fe^{3+}				0.239		0.991					0.030	0.113	0.145
Fe^{2+}	1.789	1.843	1.820	2.279	0.009		1.607	1.551	0.297	0.010	1.617	1.988	1.616
Mn	0.040	0.111	0.048	0.034	0.000	0.008	0.025	0.021	0.002	0.000	0.011	0.001	0.005
Mg	0.562	0.290	0.450	1.488	0.000	0.005	0.520	0.442	0.679	0.001	2.880	2.039	2.539
Ca	0.622	0.693	0.637	1.811	0.408	3.990	0.818	0.940	0.851	0.110	1.906	1.880	1.791
Na	0.003	0.006	0.003	0.506	0.552	0.000	0.012	0.007	0.083	0.809	0.183	0.491	0.412
K	0.000	0.000	0.000	0.117	0.003	0.000	0.001	0.001	0.000	0.004	0.043	0.263	0.140
Total	7.998	7.969	7.973	15.503	4.982	15.987	7.988	7.984	4.000	4.954	15.140	15.666	15.383

(*continued*)

TABLE 3-2. COMPOSITIONS OF MINERALS FROM GARNET AMPHIBOLITE WITH GABBROIC PROTOLITH (*continued*)

Sample No.:	HY7D	HY11A							HY11D				
Mineral:	Ilm	Grt	Zo	Pl	Ms	Amp	Amp	Ilm	Zo	Amp	Amp	Pl	Ms
Texture:			needle									pse	
SiO_2	0.03	38.29	39.36	60.76	48.57	51.82	48.34	0.05	39.18	45.90	46.24	65.83	49.21
TiO_2	52.37	0.04	0.01	0.00	0.00	0.29	0.53	52.43	0.19	0.41	0.96	0.00	0.01
Cr_2O_3	0.04	0.07	0.02	0.03	0.00	0.05	0.09	0.08	0.00	0.04	0.12	0.02	0.00
Al_2O_3	0.03	21.10	29.26	24.54	39.19	3.15	7.40	0.03	29.16	12.57	12.17	22.00	39.04
FeO	44.53	28.75	5.27	0.32	0.15	15.64	17.25	46.05	5.67	14.62	8.93	0.02	0.16
MnO	0.97	1.23	0.07	0.05	0.02	0.07	0.05	0.29	0.08	0.20	0.01	0.00	0.01
MgO	0.35	3.31	0.05	0.00	0.02	13.21	10.85	0.37	0.04	10.61	14.78	0.00	0.20
CaO	0.07	7.51	23.86	6.39	0.07	11.87	11.57	0.00	24.31	11.87	12.12	2.45	0.07
Na_2O	0.05	0.05	0.04	7.41	0.21	0.43	1.01	0.03	0.03	1.25	1.76	10.18	0.30
K_2O	0.00	0.01	0.03	0.06	8.88	0.12	0.25	0.00	0.00	0.31	0.89	0.05	9.11
Total	98.44	100.34	97.44	99.56	97.10	96.65	97.32	99.32	98.08	97.79	97.98	100.55	98.11
Si	0.001	3.024	6.067	2.711	3.096	7.630	7.154	0.001	6.017	6.704	6.622	2.876	3.110
Ti	1.006	0.002	0.001	0.000	0.000	0.032	0.059	0.999	0.022	0.045	0.103	0.000	0.000
Cr	0.001	0.004	0.002	0.001	0.000	0.006	0.011	0.002	0.000	0.005	0.014	0.001	0.000
Al	0.001	1.965	5.316	1.290	2.945	0.547	1.291	0.001	5.278	2.164	2.055	1.133	2.908
Fe^{3+}	0.000		0.611			0.135	0.170		0.655	0.132	0.069		
Fe^{2+}	0.951	1.900		0.012	0.008	1.791	1.965	0.976		1.654	1.000	0.001	0.008
Mn	0.016	0.064	0.007	0.001	0.001	0.009	0.006	0.005	0.008	0.025	0.001	0.000	0.000
Mg	0.013	0.389	0.011	0.000	0.002	2.899	2.393	0.014	0.009	2.310	3.155	0.000	0.019
Ca	0.002	0.635	3.942	0.305	0.005	1.873	1.835	0.000	4.001	1.858	1.860	0.115	0.005
Na	0.002	0.008	0.010	0.641	0.025	0.123	0.290	0.001	0.008	0.354	0.489	0.862	0.037
K	0.000	0.001	0.006	0.003	0.722	0.023	0.047	0.000	0.000	0.058	0.163	0.003	0.734
Total	1.994	7.993	15.975	4.966	6.805	15.068	15.221	1.999	15.998	15.309	15.531	4.990	6.822

(*continued*)

TABLE 3-2. COMPOSITIONS OF MINERALS FROM GARNET AMPHIBOLITE WITH GABBROIC PROTOLITH (*continued*)

Sample No.:	HY11D			HY12F					
Mineral:	Ms	Ilm	Ttn	Grt	Grt	Pl	Zo	Amp	Amp
Texture:				crn-amp	crn-pl		needle	af cpx	
SiO_2	54.90	0.02	30.85	38.60	39.06	52.95	39.51	50.26	49.40
TiO_2	0.02	53.56	38.67	0.03	0.00	0.00	0.07	0.06	0.14
Cr_2O_3	0.05	0.00	0.00	0.00	0.00	0.00	0.05	0.02	0.01
Al_2O_3	31.33	0.00	0.88	21.91	21.75	30.37	29.20	5.75	6.52
FeO	0.36	41.76	0.13	27.33	27.09	0.01	6.58	15.24	17.47
MnO	0.00	2.57	0.06	1.06	1.14	0.00	0.03	0.11	0.12
MgO	0.17	0.13	0.00	3.09	2.13	0.00	0.07	12.38	11.21
CaO	1.02	0.08	29.02	8.64	10.61	12.81	23.90	11.35	11.50
Na2O	2.29	0.03	0.00	0.00	0.02	4.10	0.00	1.04	0.99
K2O	6.55	0.00	0.00	0.00	0.00	0.03	0.02	0.18	0.21
Total	96.69	98.15	99.28	100.66	101.80	100.27	99.43	96.39	97.57
Si	3.484	0.001	1.010	3.019	3.033	2.389	6.023	7.416	7.279
Ti	0.001	1.028	0.952	0.002	0.000	0.000	0.008	0.007	0.016
Cr	0.003	0.000	0.000	0.000	0.000	0.000	0.006	0.002	0.001
Al	2.344	0.000	0.034	2.020	1.991	1.615	5.247	1.000	1.133
Fe^{3+}							0.755	0.148	0.206
Fe^{2+}	0.019	0.891	0.004	1.788	1.759	0.000		1.733	1.947
Mn	0.000	0.043	0.001	0.055	0.058	0.000	0.003	0.014	0.015
Mg	0.016	0.005	0.000	0.360	0.247	0.000	0.016	2.722	2.462
Ca	0.069	0.002	1.018	0.724	0.883	0.619	3.904	1.795	1.816
Na	0.282	0.001	0.000	0.000	0.003	0.359	0.000	0.298	0.283
K	0.530	0.000	0.000	0.000	0.000	0.002	0.004	0.034	0.040
Total	6.748	1.972	3.020	7.969	7.973	4.984	15.966	15.169	15.198

TABLE 4. MINERAL COMPOSITIONS OF GNEISS AND AMPHIBOLITE INTERLAYER

Sample No.:	HY3				HY5E			HY7B			HY17A		
Mineral:	Pl	Kfs	Kfs	Pl	Pl	Pl	Amp	Pl	Pl	Amp	Grt	Amp	Cum
Texture:	host	exs	host	exs									
SiO_2	60.26	64.13	63.00	61.56	63.23	58.65	41.74	63.29	59.88	42.52	37.31	43.43	52.33
TiO_2	0.00	0.00	0.13	0.00	0.01	0.00	0.55	0.00	0.00	0.77	0.02	0.70	0.06
Cr_2O_3	0.00	0	0.00	0.07	0.00	0.00	0.00	0.04	0.00	0.01	0.00	0.02	0.01
Al_2O_3	24.41	18.19	18.53	23.03	22.26	25.33	13.51	21.99	25.17	12.39	21.07	12.30	1.50
FeO	0.02	0.00	0.16	0.07	0.09	0.03	16.80	0.16	0.12	16.67	31.10	16.11	23.87
MnO	0.02	0.00	0.00	0.01	0.00	0.00	0.14	0.00	0.02	0.27	1.04	0.09	0.21
MgO	0.00	0.00	0.00	0.03	0.01	0.00	9.14	0.00	0.00	9.24	3.22	9.89	15.94
CaO	5.58	0.00	0.00	3.95	2.91	6.72	10.73	3.98	6.49	11.62	5.62	10.77	1.11
Na_2O	8.41	0.78	0.94	9.42	9.52	7.76	2.07	8.80	7.14	1.90	0.01	1.72	0.18
K_2O	0.21	16.23	15.72	0.15	0.35	0.06	0.37	0.12	0.09	0.68	0.01	0.45	0.00
Total	98.91	99.33	98.48	98.29	98.36	98.55	95.05	98.38	98.91	96.07	99.40	95.47	95.19
Si	2.709	2.991	2.964	2.775	2.834	2.653	6.363	2.836	2.687	6.470	2.996	6.551	7.886
Ti	0.000	0.000	0.005	0.000	0.000	0.000	0.064	0.000	0.000	0.088	0.001	0.079	0.007
Cr	0.000	0.000	0.000	0.002	0.000	0.000	0.000	0.001	0.000	0.001	0.000	0.002	0.001
Al	1.293	1.000	1.028	1.224	1.176	1.350	2.429	1.162	1.331	2.223	1.994	2.188	0.266
Fe^{3+}							0.334			0.114		0.304	
Fe^{2+}	0.001	0.000	0.006	0.003	0.003	0.001	1.808	0.006	0.005	2.007	2.089	1.728	3.008
Mn	0.001	0.000	0.000	0.000	0.000	0.000	0.018	0.000	0.001	0.035	0.055	0.012	0.021
Mg	0.000	0.000	0.000	0.002	0.001	0.000	2.078	0.000	0.000	2.095	0.385	2.222	3.581
Ca	0.269	0.000	0.000	0.191	0.140	0.326	1.754	0.191	0.312	1.894	0.484	1.741	0.179
Na	0.733	0.071	0.086	0.823	0.827	0.681	0.613	0.765	0.621	0.561	0.002	0.503	0.051
K	0.012	0.966	0.944	0.009	0.020	0.003	0.072	0.007	0.005	0.132	0.001	0.087	0.000
Total	5.017	5.027	5.032	5.028	5.001	5.014	15.533	4.968	4.961	15.620	8.007	15.419	14.999

(*continued*)

TABLE 4. MINERAL COMPOSITIONS OF GNEISS AND AMPHIBOLITE INTERLAYER (*continued*)

Sample No.:	HY17A	HY19A				
Mineral:	Pl	Grt	Amp	Pl	Pl	Ttn
Texture:						
SiO_2	63.29	38.16	42.37	59.79	56.72	30.39
TiO_2	0.00	0.02	0.86	0.03	0.00	39.19
Cr_2O_3	0.04	0.01	0.00	0.00		0.01
Al_2O_3	21.99	21.30	13.16	25.05	26.78	0.96
FeO	0.16	25.06	17.00	0.00	0.04	0.29
MnO	0.00	1.91	0.12	0.00	0.02	0.03
MgO	0.00	2.05	8.48	0.00	0.01	0.00
CaO	3.98	12.08	11.31	6.12	8.43	28.79
Na_2O	8.80	0.00	1.79	8.01	6.83	0.02
K_2O	0.12	0.01	0.36	0.06	0.05	0.00
Total	98.38	100.57	95.45	99.06	98.88	99.68
Si	2.836	3.008	6.462	2.683	2.570	0.996
Ti	0.000	0.001	0.099	0.001	0.000	0.966
Cr	0.001	0.000	0.000	0.000	0.000	0.000
Al	1.162	1.979	2.366	1.325	1.430	0.037
Fe^{3+}	0.000	0.000	0.137	0.000	0.000	0.000
Fe^{2+}	0.006	1.652	2.031	0.000	0.002	0.008
Mn	0.000	0.099	0.016	0.000	0.001	0.001
Mg	0.000	0.240	1.928	0.000	0.001	0.000
Ca	0.191	1.020	1.848	0.294	0.409	1.011
Na	0.765	0.000	0.529	0.697	0.600	0.001
K	0.007	0.001	0.070	0.003	0.003	0.000
Total	4.968	8.001	15.487	5.004	5.016	3.020

TABLE 5. COMPOSITIONS OF AMPHIBOLES FROM GRANULITE AND METAGABBRO

Sample No.:	HY12A			HY12B					03-R14				HY15E
Texture:	Amp1	in cpx	af opx	Amp1	Amp1	Ia in cpx	Amp2	Amp2	Amp1	Amp2	Amp2	Amp2	inc
SiO_2	44.06	46.71	54.38	44.42	46.24	44.96	50.94	51.60	43.50	43.95	53.92	53.71	41.13
TiO2	1.56	0.86	0.14	1.32	0.96	1.05	0.41	0.42	1.04	0.85	0.03	0.18	0.91
Cr_2O_3	0.15	0.09	0.04	0.16	0.12	0.07	0.00	0.05	0.01	0.01	0.00	0.01	0.05
Al_2O_3	13.85	10.88	3.31	13.43	12.17	12.36	7.52	5.53	14.24	13.54	0.54	2.94	14.98
FeO	9.90	10.56	8.25	9.30	8.93	12.73	8.12	8.62	12.39	12.43	24.67	14.22	17.51
MnO	0.04	0.00	0.02	0.04	0.01	0.12	0.09	0.06	0.09	0.03	0.05	0.07	0.03
MgO	12.94	13.34	18.07	13.47	14.78	11.77	17.92	17.37	11.02	10.98	16.84	15.96	8.53
CaO	11.71	12.33	12.10	11.78	12.12	11.95	11.23	11.80	11.88	11.63	1.00	10.23	11.10
Na_2O	1.78	1.47	0.42	1.88	1.76	2.40	1.45	1.08	1.33	1.10	0.09	0.35	1.86
K_2O	1.41	0.83	0.10	1.23	0.89	0.03	0.02	0.34	1.29	1.32	0.04	0.15	1.53
Total	97.40	97.06	96.83	97.03	97.98	97.46	97.69	96.87	96.80	95.85	97.18	97.81	97.64
Si	6.417	6.802	7.703	6.470	6.622	6.592	7.131	7.353	6.440	6.546	7.960	7.719	6.183
Ti	0.171	0.094	0.015	0.145	0.103	0.116	0.043	0.045	0.115	0.096	0.004	0.020	0.103
Cr	0.017	0.010	0.005	0.018	0.014	0.008	0.000	0.006	0.002	0.001	0.000	0.002	0.006
Al	2.378	1.868	0.553	2.306	2.055	2.136	1.241	0.929	2.486	2.377	0.094	0.498	2.655
Fe^{3+}	0.007	0.000	0.063	0.005	0.069	0.000	0.206	0.098	0.001	0.018	0.000	0.000	0.114
Fe^{2+}	1.199	1.286	0.914	1.128	1.000	1.561	0.540	0.831	1.514	1.512	3.046	1.709	1.973
Mn	0.005	0.000	0.002	0.005	0.001	0.015	0.010	0.007	0.012	0.004	0.006	0.008	0.004
Mg	2.809	2.895	3.815	2.924	3.155	2.572	3.740	3.689	2.433	2.438	3.705	3.419	1.912
Ca	1.827	1.924	1.837	1.839	1.860	1.877	1.684	1.802	1.885	1.856	0.159	1.576	1.789
Na	0.503	0.415	0.115	0.531	0.489	0.682	0.393	0.298	0.382	0.318	0.024	0.096	0.541
K	0.262	0.154	0.018	0.229	0.163	0.007	0.004	0.061	0.243	0.250	0.007	0.027	0.293
Total	15.595	15.448	15.040	15.600	15.531	15.566	14.992	15.118	15.512	15.417	15.005	15.073	15.572

(*continued*)

TABLE 5. COMPOSITIONS OF AMPHIBOLES FROM GRANULITE AND METAGABBRO *(continued)*

Sample No.:	HY1A				HY1B			HY12G		
Texture:	Amp1	Amp2	Amp2	Amp2	Amp1	Amp2	Amp2	Amp2	Amp2	af opx
SiO_2	38.50	47.58	51.05	44.06	40.23	45.94	52.74	52.54	53.09	47.54
TiO_2	2.01	0.85	0.39	1.10	1.72	0.51	0.14	0.23	0.09	0.74
Cr_2O_3	0.03	0.04	0.04	0.03	0.12	0.10	0.10	0.07	0.02	0.03
Al_2O_3	12.97	7.82	4.73	10.85	12.46	9.30	1.28	3.21	2.24	7.82
FeO	22.53	16.54	17.29	17.59	21.30	18.99	23.85	12.60	17.64	14.59
MnO	0.13	0.07	0.11	0.09	0.08	0.09	0.15	0.05	0.30	0.07
MgO	5.72	11.23	13.42	10.25	6.70	9.47	14.27	15.71	12.83	12.79
CaO	11.04	11.01	9.71	11.06	11.30	11.26	4.23	11.71	11.40	11.04
Na_2O	1.67	1.13	0.42	1.81	1.86	1.39	0.19	0.50	0.34	1.40
K_2O	2.43	0.66	0.31	0.93	2.11	0.64	0.08	0.13	0.02	0.38
Total	97.03	96.93	97.47	97.77	97.85	97.66	97.03	96.75	97.97	96.40
Si	6.071	7.058	7.475	6.569	6.225	6.868	7.869	7.604	7.762	7.017
Ti	0.238	0.095	0.043	0.123	0.200	0.058	0.016	0.025	0.010	0.082
Cr	0.004	0.005	0.005	0.004	0.015	0.012	0.012	0.008	0.002	0.004
Al	2.398	1.368	0.817	1.907	2.273	1.637	0.225	0.548	0.386	1.361
Fe^{3+}	0.158	0.238	0.124	0.300	0.089	0.113		0.183	0.097	0.303
Fe^{2+}	2.814	1.814	1.993	1.893	2.668	2.139	2.976	1.342	2.060	1.498
Mn	0.017	0.009	0.014	0.011	0.011	0.011	0.015	0.006	0.037	0.009
Mg	1.344	2.483	2.928	2.278	1.545	2.109	3.174	3.388	2.796	2.813
Ca	1.866	1.750	1.523	1.767	1.874	1.804	0.676	1.816	1.786	1.746
Na	0.511	0.325	0.119	0.523	0.558	0.403	0.055	0.140	0.096	0.401
K	0.489	0.125	0.058	0.177	0.417	0.122	0.015	0.024	0.004	0.072
Total	15.910	15.270	15.099	15.552	15.875	15.273	15.032	15.084	15.967	15.306

Note: Ferric iron for calcic amphibole was calculated using a procedure by Schumacher (1991). HY12A–HY15E: granulite; others: metagabbro. af opx: after opx; la: lamellae; inc: inclusion.

TABLE 6. MINERAL COMPOSITIONS OF METAMORPHIC MAFIC AND GRANITIC DIKES

Sample No:	HY19B							HY7H				
Mineral:	Grt	Grt	Amp	Zo	Pl	Ilm	Ttn	Pl	Kfs	Bt	Ms	Grt
SiO_2	38.67	38.47	42.02	38.83	57.78	0.02	31.01	64.00	63.00	34.51	45.14	36.31
TiO_2	0.02	0.05	0.79	0.20	0.02	51.55	38.50	0.00	0.00	3.08	0.91	0.02
Cr_2O_3	0.01	0.04	0.02	0.00	0.01	0.01	0.00	0.00	0.00	0.00	0.01	0.00
Al_2O_3	21.28	21.31	15.02	29.65	26.31	0.00	1.14	22.33	18.73	16.55	28.36	20.67
FeO	23.42	23.96	16.22	4.54	0.11	44.03	0.16	0.00	0.00	25.11	5.65	24.51
MnO	3.48	3.30	0.14	0.03	0.00	0.90	0.00	0.00	0.00	0.33	0.02	13.60
MgO	2.24	2.24	8.25	0.06	0.01	0.91	0.00	0.00	0.00	4.88	1.35	0.63
CaO	11.37	10.76	11.26	23.01	8.22	0.64	27.02	3.11	0.01	0.03	0.00	4.00
Na_2O	0.01	0.03	1.42	0.01	6.51	0.02	0.01	9.68	1.02	0.11	0.19	0.04
K_2O	0.00	0.00	1.19	0.00	0.10	0.00	0.00	0.30	14.99	9.10	10.92	0.00
Total	100.50	100.16	96.33	96.33	99.07	98.08	97.84	99.42	97.75	93.70	92.55	99.75
Si	3.032	3.028	6.359	6.035	2.606	0.001	1.028	2.838	2.970	2.762	3.189	3.028
Ti	0.001	0.003	0.090	0.023	0.001	0.992	0.957	0.000	0.000	0.185	0.048	0.001
Cr	0.000	0.002	0.002	0.000	0.000	0.000	0.000	0.000	0.000	0.000	0.001	0.000
Al	1.966	1.977	2.679	5.432	1.399	0.000	0.044	1.167	1.041	1.561	2.361	2.031
Fe^{total}	1.535	1.577	2.053	0.590	0.004	0.942	0.004	0.000	0.000	1.689	0.335	1.709
Mn	0.231	0.220	0.018	0.003	0.000	0.019	0.000	0.000	0.000	0.018	0.001	0.749
Mg	0.262	0.263	1.861	0.014	0.001	0.035	0.000	0.000	0.000	0.582	0.142	0.078
Ca	0.955	0.907	1.826	3.832	0.397	0.018	0.957	0.148	0.001	0.003	0.000	0.357
Na	0.002	0.004	0.417	0.003	0.569	0.001	0.001	0.832	0.093	0.017	0.026	0.006
K	0.000	0.000	0.230	0.000	0.006	0.000	0.000	0.017	0.902	0.929	0.984	0.000
Total	7.984	7.981	15.534	15.932	4.983	2.008	2.991	5.003	5.007	7.745	7.087	7.958

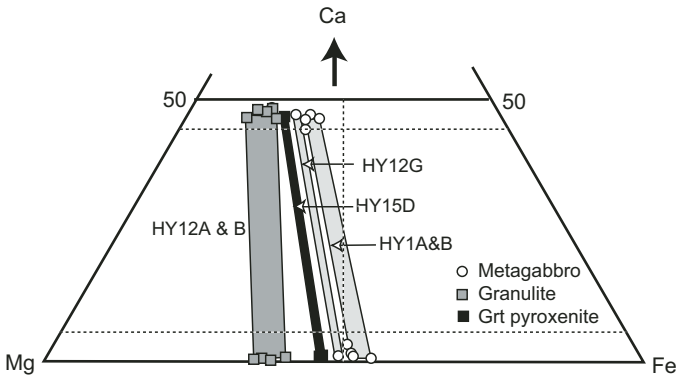

Figure 10. Compositional plots of representative clinopyroxene and orthopyroxene from granulite, metagabbro, and garnet pyroxenite.

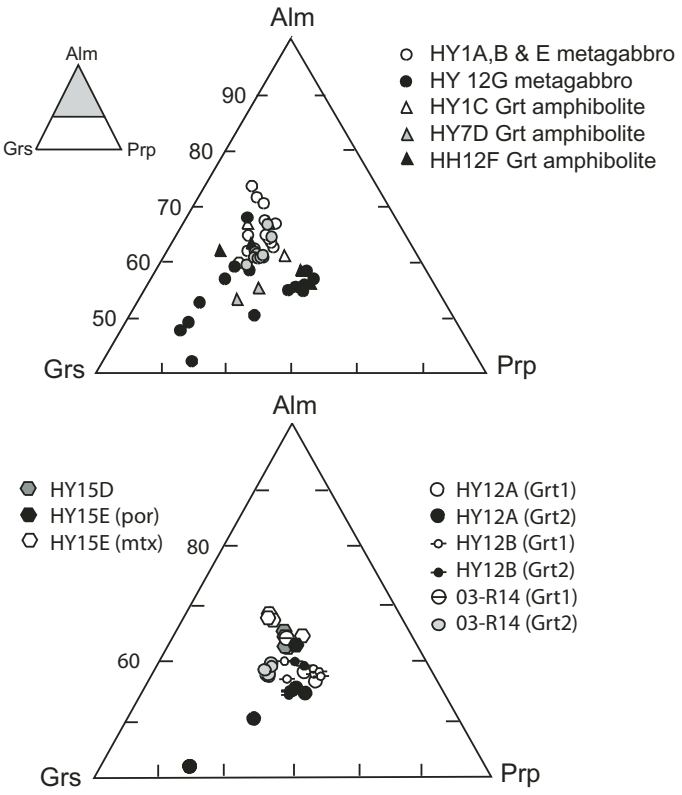

Figure 11. Almandine (Alm)-grossular (Grs)-pyrope (Prp) compositional plots of garnets from metagabbro and garnet amphibolite with gabbro protolith (A) and granulite (B). mtx—matrix; por—porphyroblast.

Plagioclase

Primary plagioclase (Pl_1) is only locally preserved in incipiently metamorphosed gabbro; most Pl_1 have been replaced by Pl_2 + Zo ± Grt ± Ms + An (pseudomorph after Pl_1) in granulite, and by Pl_2 + Zo ± Ky ± Grt + An in metagabbro. Only minor relict Pl_1 spots were analyzed (e.g., metagabbro HY1E, which has An_{55}). Pl_2 crystals are both calcic ($An_{50–77}$) and sodic ($An_{21–36}$) with gradational boundaries. Minor anorthite laths ($An_{>90}$) occur in plagioclase pseudomorphs after Pl_1. Most plagioclase from garnet amphibolite is sodic ($Ab_{36–88}$).

METAMORPHIC REACTIONS AND *P-T* CONDITIONS

Mineral reaction textures record *P-T*-assemblage evolution. The most common coronas observed in this study contain two layers of $|\text{Amp} \pm \text{Qtz}|\text{Grt}|$ or a single layer of garnet separating pyroxene (clinopyroxene or orthopyroxene) from plagioclase, and define the following reactions:

$$\text{Cpx} + \text{Pl} + \text{H}_2\text{O} = \text{Hbl} + \text{Qtz} + \text{Grt}, \quad (1)$$

$$\text{Opx} + \text{Cpx} + \text{Pl} + \text{H}_2\text{O} = \text{Hbl} + \text{Grt} + \text{Qtz}, \quad (2)$$

$$\text{Cpx} + \text{Pl} = \text{Grt}. \quad (3)$$

The coronae of $|\text{Grt}_2|\text{Amp} + \text{Qtz}|$ that separate garnet (Gr_1) from clinopyroxene define the reaction:

$$\text{Grt}_1\ (\text{Alm-rich}) + \text{Cpx} + \text{H}_2\text{O} = \text{Grt}_2\ (\text{Grs-rich}) + \text{Amp} + \text{Qtz}. \quad (4)$$

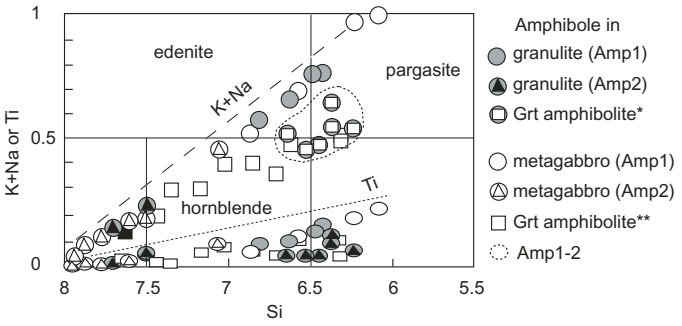

Figure 12. Si versus (Na + K) and Si versus Ti plots of amphiboles from granulite, metagabbro, and garnet amphibolite. Amp_1 from metagabbro and granulite have high contents of Ti and (Na + K) in p.f.u. Amphiboles include actinolite and cummingtonite in the field of Na + K < 0.5 and Si > 7.5; others are calcic amphibole (Ca_B > 1.5). * and ** represent garnet amphibolites with minor relict Amp_1 derived from granulite and gabbro, respectively.

In metagabbro, the reactions forming $|\text{Grt}|\text{Amp} + \text{Qtz}|$ coronae between plagioclase and pyroxene may follow the same reactions 1, 2, and 3. Plagioclase is replaced by fine-grained assemblages of Zo + Pl_2 + Ky ± An + Qtz ± Grt. Zoisite, Pl_2, minor Ky, and An are the main products; grossular-rich garnet is only locally developed. These newly grown crystals are randomly distributed and coarsen with advanced recrystallization. Plagioclase breakdown in a closed system is a function of pressure (Goldsmith, 1982) and can be approximated by the following reactions:

$$Pl + H_2O \rightarrow Zo + Ky + Qtz + (NaSiCa_{-1}Al_{-1})_{Pl} \text{ and} \quad (5)$$

$$Pl \rightarrow Grt + Ky + Qtz + (NaSiCa_{-1}Al_{-1})_{Pl} \quad (6)$$

The process can be more complex and involve reactions with mafic minerals.

As described above, most pyroxenes underwent exsolution and reaction with plagioclase. The compositions of the original minerals in the Haiyangsuo granulite may have been modified to various extents, hence estimating *P-T* conditions based on mineral compositions is a difficult task. Only the compositions of less-altered minerals were used to estimate *P-T* conditions. Metamorphic pressures and temperatures of granulites were calculated at 800, 700, and 600 °C, and 5, 10, and 15 kbar (see Table 7-1). The Grt-Opx (Wood, 1974; Harley and Green, 1982) and Grt-Cpx-Opx-Pl-Qtz barometers (Paria et al., 1988) were employed to estimate pressure, and yielded 10 ± 1 kbar at 700 °C. The Grt-Cpx (Powell, 1985) and Grt-Opx thermometers (Harley, 1984) yielded similar temperatures of 605–665 °C at 10 kbar. The Opx-Cpx thermometer (Wood and Banno, 1973) independently gave higher temperature of 740–805 °C for coarse-grained Cpx and Opx from samples HY12A and HY15D; the clinopyroxene host and exsolved orthopyroxene lamellae yielded 650–730 °C (average 690 °C). These estimates represent post-peak equilibration after exsolution, because high cation-diffusion rates generally preclude the preservation of early, prograde, or maximum-*T* segments of a *P-T* path (Harley, 1989). The metamorphic temperature of the granulite-facies recrystallization was likely higher than the temperature obtained from clinopyroxene with orthopyroxene exsolution lamellae (>690 °C).

Amphibole-plagioclase thermometry (Blundy and Holland, 1990; Holland and Blundy, 1994) and Hbl-Grt-Pl thermobarometry (Dale et al., 2000) were employed to estimate *P-T* conditions for the Haiyangsuo garnet amphibolites, including the various gabbro and mafic dike protoliths. In these calibrations, both garnet and amphibole were assumed to obey a regular solution model; plagioclase was modeled using the expressions in Holland and Powell (1992). As shown in Table 7, the average recrystallization temperatures of T_A (Ed + 4Qtz = Tr + Ab) and T_B (Ed + Ab = richterite + Act) were 725, 685, and 655 °C for metamafic dike HY19B, and 545–680, 550–655, and 555–645 °C for metagabbro, at 10, 8, and 6 kbar, respectively. Sample HY19B is a completely recrystallized amphibolite, which is consistent with a higher-*T* estimate. The most-recrystallized metagabbros have higher temperature estimates than those in which plagioclase pseudomorphs are preserved. Pressure estimates range from 6.5 to 11 kbar at 600 °C.

DISCUSSION

Granulite *P-T-t* Path and Its Possible Origin

The U-Pb SHRIMP dating of zircons from the present study and that of Chu (2005) yielded the following results. The Haiyangsuo granulite experienced two recrystallization events: (1) granulite-facies recrystallization at 1846 ± 26 Ma, and (2) an amphibolite-facies overprint at 373 ± 65 Ma. Emplacement of the gabbro intrusions occurred at 1734 ± 5 Ma, and the amphibolite-facies recrystallization of the metagabbro was at 339 ± 59 Ma. The amphibolite-facies recrystallization of both granulite and gabbro produced identical corona textures, and has a similar age within uncertainty, suggesting that both resulted from one tectonometamorphic event. Based on the observed textures, age data, and *P-T* estimates described in the previous sections, the Haiyangsuo granulites show a near-isobaric cooling (IBC) *P-T-t* path (Fig. 13).

Ye et al. (1999) described a fine-grained diopside ± omphacite assemblage around the edges of relict clinopyroxene porphyroblasts, and suggested that the granulites recrystallized during compression from the granulite to the eclogite stability field. The Grt + Di + Pl paragenesis is also present in local domains in plagioclase from our granulite and metagabbro samples. In general, the Grt + Cpx + Pl ± Qtz assemblage represents a paragenetic link between a plagioclase-free eclogite-facies metabasite and an orthopyroxene-bearing granulite-facies metabasite, and the Grt + Cpx + Pl paragenesis occurs in local domains in plagioclase of the Haiyangsuo granulite and metagabbro. However, this assemblage may also occur in lower amphibolite–facies rocks (Fig. 13B) and is not definitive of high-*P* granulite (Pattison, 2003).

In fact, omphacite with a measurable Jd (~24 mol%) component was encountered only in one analysis in the Haiyangsuo granulite (Ye et al., 2000); more than 99% of the coronal assemblages between pyroxene and plagioclase were │Amp ± Qtz│Grt│ or garnet rather than omphacite-garnet. Even though a transitional eclogite *P-T* field has been suggested for these rocks, isobaric cooling can also explain such a transition. Holland and Powell (1998, Fig. 8) proposed a *P-T* pseudosection for the NCFMAS system to explain the phase relationship and *P-T* conditions of the granulite-eclogite transition. As shown in Figure 13D, the transition from a trivariant field of granulite (Grt + Cpx + Opx + Pl) to another trivariant field (Grt + Omp + Ky + Pl) and a divariant field (Grt + Omp + Cpx + Ky + Pl) can happen through either near-isobaric cooling (IBC) or increasing pressure. Granulites showing an isobaric cooling history have been considered to have formed at various origins and settings (Harley, 1989). The Haiyangsuo granulite may have been derived from a Proterozoic granulite-amphibolite terrane. The low recrystallization temperature and the counterclockwise isobaric cooling *P-T* path of the Haiyangsuo granulite may indicate formation during the thickening of extended thin crust, as proposed by Harley (1989).

Non-UHP Unit in the Sulu UHP Terrane

The whole Sulu UHP terrane (see Fig. 1) has long been considered to be a coesite-eclogite (UHP) belt in fault contact with the eclogite-free high-pressure belt in southern Sulu. The

TABLE 7-1. PRESSURE-TEMPERATURE CALCULATIONS OF GRANULITE

	T(°C)			P(kbar)		
	Opx1-Cpx1 Wood and Banno (1973)	Grt1-Cpx1 Powell (1985)	Grt1-Opx1 Harley (1984)	Grt1-Opx1 Wood (1974)	Grt1-Opx1 Harley and Green (1982)	Grt-Px-Pl Paria et al. (1988)
HY12A	740					
15/800		630	675	14.4	10	14.4
10/700		620	650	9.6	9.4	10.7
5/600		610	625	4.9	8.7	7.0
HY12B	650-730*					
15/800		680	650	14.1	9.7	15.2
10/700		665	625	9.4	9.0	11.5
5/600		655	600	4.7	8.4	7.6
HY15D	805					
15/800				17.8	11.3	
10/700				12.5	10.7	
5/600				7.2	9.9	
HY15E						
15/800		640	630	15.4	11.8	
10/700		630	605	10.3	11.4	
5/600		615	580	5.2	10.5	

Note: Temperature and pressure were calculated at 15, 10, and 5 kbar, and at 800, 700, and 600 °C, respectively.
*host Cpx - exsolved Opx

TABLE 7-2. PRESSURE-TEMPERATURE CALCULATIONS OF GARNET AMPHIBOLITE

	T (°C)				P (kbar)			
Sample	Grt-Hbl GR(1984) (Graham and Powell,1984)	Amp-Pl (Blundy and Holland, 1990)	Amp-Pl at 10 kbar (Holland and Blundy, 1994)		Grt-Pl-Amp at 600°C (Dale et al., 2000)			Pl-Amp (Blundy and Holland,1990)
			Ta metagabbro	Tb	P1	P2	P3	
HY1C	891	752	687	653	12.8	12.4	12.1	10
HY12F	557	596	623	687	6.7	7.4	7.7	1.9
HY19B	666	744	769	655	11	10.4	11.6	9.9

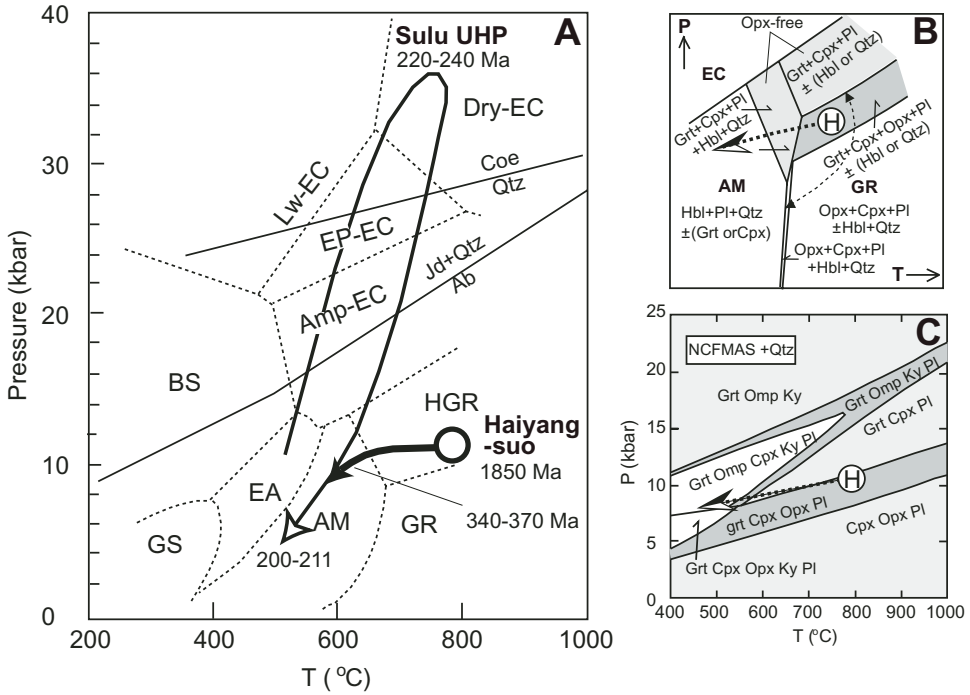

Figure 13. (A) Estimated pressure-temperature-time (*P-T-t*) path of the Haiyangsuo granulite showing near-isobaric cooling (IBC) history. For comparison, a simplified *P-T-t* path of Sulu ultrahigh-pressure (UHP) rocks is also shown. (B) Schematic *P-T* diagram showing the *P-T* domains of granulite and amphibolite mineral assemblages modified after Pattison (2003) and the Haiyangsuo granulite near-isobaric cooling path. (C) A *P-T* pseudosection for an aluminous andesitic basalt bulk composition showing the transformation from granulite to eclogite (EC) after Holland and Powell (1998). Abbreviations are after Kretz (1983). EC—eclogite; EP—epidote; BS—blueschist; GS—greenschist, EA—epidote-amphibolite; HGR—high-P granulite; AM—amphibolite; GR—granulite.

rock association and metamorphic evolution histories in the Haiyangsuo area are different, however, from both Sulu UHP and high-pressure rocks. Ye et al. (1999) correlated the Haiyangsuo "transitional eclogite" with the "cold eclogite" of south Dabie, and interpreted the Haiyangsuo area as an equivalent to the Dabie "cold eclogite belt," which is widespread in Dabie.

The Haiyangsuo granulite, however, was overprinted by garnet amphibolite rather plagioclase-bearing "transitional eclogite" to garnet amphibolite. The presence of very rare omphacite in a plagioclase-stable terrane may simply reflect metastable growth during isobaric cooling. Furthermore, most of the zircons from Dabie-Sulu high-pressure and UHP eclogites and gneisses have Neoproterozoic cores ranging from ca. 625 to 800 Ma (Hacker et al., 2000, 2006; Liu et al., 2004b, 2005). Moreover, $^{40}Ar/^{39}Ar$ ages from the Sulu UHP rocks are ca. 220–200 Ma (Cong et al., 1992; Webb et al., this volume; Xu et al., this volume). In the Haiyangsuo area, the protoliths for the gneissic and mafic rocks—including the gabbroic intrusions—have Early Proterozoic ages; some could be Archean. The 600–800 Ma Late Proterozoic protolith ages and the Triassic high-pressure and UHP metamorphic ages common in Dabie-Sulu high-pressure and UHP rocks were not observed. Based on the geochronologic and petrological data documented above, we suggest that the Haiyangsuo granulite-amphibolite facies complex is exotic to the Sulu UHP–high-pressure terrane. However, the correlation of the Haiyangsuo unit with other tectonic terranes in eastern China and the Korean peninsula remains to be investigated.

CONCLUSION

The Haiyangsuo area exposes three lithological units: (1) gneiss with granulite lenses and amphibolite layers, (2) metagabbro, and (3) granitic dikes. Unit 1 is dominant, displays several stages of metamorphism, and has a protolith age older than 2500 Ma. The granulite (Grt + Cpx + Opx ± Pl +Ilm/Rt ± Qtz ± Prg ± Bt) is volumetrically minor; most has been retrogressed to garnet amphibolite (Grt + Hbl + Ilm + Pl ± Qtz) at the margins of the granulite lenses. Coronas of │Grt│ Qtz ± Amp│ at the contacts between plagioclase and pyroxene indicate an isobaric cooling history. A SHRIMP U-Pb age of ca. 1850 Ma for metamorphic zircon from the granulite probably represents the first metamorphic event of unit 1, when the amphibolite-facies gneiss, granulite, and garnet amphibolite layers were metamorphosed. An amphibolite-facies overprint took place at 373 ± 65 Ma. Unit 2 exhibits various extents of transformation, with

incipient corona textures in the cores of the gabbros to a garnet amphibolite along the margins. Gabbroic rocks with primary phases (Opx + Opx + Pl + Ilm ± Qtz) formed at 1734 ± 5 Ma; they were subsequently recrystallized in amphibolite facies at 339 ± 59 Ma. The amphibolite-facies recrystallization of the granulite and gabbro probably resulted from a single tectonometamorphic event. The granitic dikes are much younger (160 ± Ma) but coeval with the SHRIMP age of the Rushan granite, ~20 km farther west (Hu et al., 2004; Fig. 1). The rock associations and metamorphic history indicate that the Haiyangsuo area is exotic to the Triassic Sulu high-pressure–UHP terrane, with which it was juxtaposed in the Jurassic.

ACKNOWLEDGMENTS

This research resulted from a U.S.-China cooperative project supported by the National Science Foundation (NSF) grant EAR-0003355 and EAR-0506901. We thank F. Mazdab, R. Zhao, and K. Okamoto for their assistance in sensitive high-resolution ion microprobe (SHRIMP) and microprobe laboratories, and W. Chu for his unpublished age data and generous help. We appreciate B. Hacker, S. Wallis, M. Terry, and W.G. Ernst for their critical review and material improvement of the manuscript.

REFERENCES CITED

Ames, L., Zhou, G.Z., and Xiong, B., 1996, Geochronology and geochemistry of ultrahigh-pressure metamorphism with implications for collision of the Sino-Korean and Yangtze cratons, central China: Tectonics, v. 15, p. 472–489, doi: 10.1029/95TC02552.

Blundy, J.D., and Holland, T.J.B., 1990, Calcic amphibole equilibria and a new amphibole plagioclase geothermometer: Contributions to Mineralogy and Petrology, v. 104, p. 208–224, doi: 10.1007/BF00306444.

Chu, W., 2005, Geochronological and petrological studies of Haiyangsuo region Sulu UHP terrane, eastern China [M.S. thesis]: Stanford, Stanford University, 80 p.

Cong, B.L., Zhang, R.Y., Li, S.G., Zhai, M.G., Wang, S.S., Cheng, C.Y., and Ishiwatari, A., 1992, Preliminary study of isotope chronology of northern Jiangsu and eastern Shandong province, China, *in* Ishda, S., ed., Exploration of volcanoes and rocks in Japan, China and Antarctica: Yamaguchi, Yamaguchi University, p. 411–419.

Dale, J., Holland, T., and Powell, R., 2000, Hornblende-garnet-plagioclase thermobarometry: A natural assemblage calibration of the thermodynamics of hornblende: Contributions to Mineralogy and Petrology, v. 140, p. 353–362, doi: 10.1007/s004100000187.

Goldsmith, J.R., 1982, Plagioclase stability at elevated temperatures and pressures: The American Mineralogist, v. 66, p. 1183–1188.

Harley, S.L., 1984, An experimental study of the partitioning of Fe-Mg between garnet and orthopyroxene: Contributions to Mineralogy and Petrology, v. 86, p. 359–373, doi: 10.1007/BF01187140.

Harley, S.L., 1989, The origins of granulites: A metamorphic perspective: Geological Magazine, v. 126, p. 215–247.

Harley, S.L., and Green, D.H., 1982, Garnet-orthopyroxene barometry for granulite and peridotites: Nature, v. 300, p. 697–701, doi: 10.1038/300697a0.

Hacker, B.R., Ratschbacher, L., Webb, L., McWilliams, M.O., Ireland, T., Calvet, A., Dong, S., Wenk, H.R., and Chateigner, D., 2000, Exhumation of ultrahigh-pressure continental crust in east central China: Journal of Geophysical Research, v. 105, p. 13,339–13,364, doi: 10.1029/2000JB900039.

Hacker, B.R., Wallis, S., Grove, M., and Gehrels, G., 2006, U-Pb SIMS and LA-ICP-MS zircon and monazite ages constrain the architecture of the ultrahigh-pressure Sulu orogen: Tectonics (in press).

Han, Z., Zhang, G., Guo, H., Zhang, Z., and Wang, L., 1993, Sm-Nd isochronism age of eclogite from southern Shandong province and its tectonics significance: Journal of Ocean University of Qingdao, v. 23, p. 120–124.

Hirajima, T., Ishiwatari, A., Cong, B.L., Zhang, R.Y., Banno, S., and Nozaka, T., 1990, Identification of coesite in Mengzhong eclogite from Donghai county, northeastern Jiangsu province, China: Mineralogical Magazine, v. 54, p. 579–584.

Holland, T., and Blundy, J., 1994, Non-ideal interactions in calcic amphiboles and their bearing on amphibole-plagioclase thermometry: Contributions to Mineralogy and Petrology, v. 116, p. 433–447, doi: 10.1007/BF00310910.

Holland, T.J.B., and Powell, R., 1992, Plagioclase feldspars: Activity-composition relations based upon Darken's Quadratic Formalism and Landau theory: The American Mineralogist, v. 77, p. 53–61.

Holland, T., and Powell, R., 1998, An internally consistent thermodynamic data set for phases of petrological interest: Journal of Metamorphic Geology, v. 16, p. 309–343, doi: 10.1111/j.1525-1314.1998.00140.x.

Hu, F., Fang, H., Yang, J., Wan, Y., Liu, D., Zhai, M., and Jin, C., 2004, Mineralizing age of the Rushan Iode gold deposit in the Jiaodong Peninsula: SHRIMP U-Pb dating on hydrothermal zircon: Chinese Science Bulletin, v. 49, p. 1629–1636, doi: 10.1360/04wd0105.

Kretz, R., 1983, Symbols for rock-forming minerals: The American Mineralogist, v. 68, p. 277–279.

Li, S., Xiao, Y., Liou, D., Chen, Y., Ge, N., Zhang, Z., Sun, S-S., Cong, B., Zhang, R., Hart, S.R., and Wang, S., 1993, Collision of the North China and Yangtze blocks and formation of coesite-bearing eclogite: Timing and processes: Chemical Geology, v. 109, p. 89–111, doi: 10.1016/0009-2541(93)90063-O.

Li, S., Chen, Y., Song, M., Zhang, Z., Yang, C., and Zhao, D., 1994, U-Pb zircon ages of amphibolite from the Haiyangsuo area, eastern Shandong Province: An example for influence of multi-metamorphism to lower and upper intercepts of zircon discordia line at the concordia curve: Acta Geoscientia Sinica, v. 12, p. 37–42 (in Chinese with English abstract).

Liu, F., Xu, Z., and Liou, J.G., 2004a, Tracing the boundaries between UHP and HP metamorphic belts in southwestern Sulu region, eastern China: Evidence from mineral inclusions in zircons from metamorphic rocks: International Geology Review, v. 46, p. 409–452.

Liu, F., Xu, Z., and Liou, J.G., 2004b, SHRIMP U-Pb ages of ultrahigh-pressure and retrograde metamorphism of gneisses from southwestern Sulu terrane, eastern China: Journal of Metamorphic Geology, v. 22, p. 315–326, doi: 10.1111/j.1525-1314.2004.00516.x.

Liu, F., Liou, J.G., and Xu, Z., 2005, U-Pb SHRIMP ages recorded in the coesite-bearing zircon domains of paragneisses in the southwestern Sulu terrane, eastern China: New interpretation: The American Mineralogist, v. 90, p. 790–800, doi: 10.2138/am.2005.1677.

Ludwig, K.R., 2001, SQUID 1.02: Berkeley Geochronology Center Special Publication 2, 19 p.

Ludwig, K.R., 2003, Isoplot 3: Berkeley Geochronology Center Special Publication 4, 70 p.

Paria, P., Bhattacharya, A., and Sen, S.K., 1988, The reaction garnet + clinopyroxene + quartz = 2 orthopyroxene + anorthite: A potential geobarometer for granulites: Contributions to Mineralogy and Petrology, v. 99, p. 126–133, doi: 10.1007/BF00399372.

Pattison, D.R.M., 2003, Petrogenetic significance of orthopyroxene-free garnet + clinopyroxene + plagioclase ± quartz-bearing metabasites with respect to the amphibolite and granulite facies: Journal of Metamorphic Geology, v. 21, p. 21–24, doi: 10.1046/j.1525-1314.2003.00415.x.

Powell, R., 1985, Regression diagnostic and robust regression in geothermometer/geobarometer calibration: The garnet-clinopyroxene geothermometer revisited: Journal of Metamorphic Geology, v. 3, p. 231–243.

Schumacher, J.C., 1991, Empirical ferric iron corrections: Necessity, assumptions and effects on selected geothermobarometers: Mineralogical Magazine, v. 55, p. 3–18.

Wallis, S., Enami, M., and Banno, S., 1999, The Sulu UHP terrane: A review of the petrology and structural geology: International Geology Review, v. 41, p. 906–920.

Wallis, S., Tsuboi, M., Suzuki, K., Fanning, M., Jiang, L., and Tanaka, T., 2005, Role of partial melting in the evolution of the Sulu (eastern China) ultrahigh-pressure terrane: Geology, v. 33, p. 129–162, doi: 10.1130/G20991.1.

Wang, R., An, J., and Lai, X., 1995, Discovery of an ophiolite suite in eastern Shandong Peninsula and its significance: Acta Petrologica Sinica, v. 11, p. 221–228.

Williams, I.S., 1998, U-Th-Pb geochronology by ion microprobe, *in* Mickibbeen, M.A., Shanks, W.C., III, and Ridley, I., eds., Application of microanalytical techniques to understanding mineralizing processes: Society of Economic Geologists Reviews in Economic Geology, v. 7, p. 1–35.

Wood, B.J., 1974, The solubility of alumina in orthopyroxene coexisting with garnet: Contributions to Mineralogy and Petrology, v. 46, p. 1–14, doi: 10.1007/BF00377989.

Wood, B.J., and Banno, S., 1973, Garnet-orthopyroxene and orthopyroxene-clinopyroxene relationships in simple and complex systems: Contributions to Mineralogy and Petrology, v. 42, p. 109–124, doi: 10.1007/BF00371501.

Yang, J.S., Wooden, J.L., Wu, C.L., Liu, F.L., Xu, Z.Q., Shi, R.D., Liou, J.G., and Maruyama, S., 2003, SHRIMP U-P dating of coesite-bearing zircon from the ultrahigh-pressure metamorphic rocks, Sulu terrane, east China: Journal of Metamorphic Geology, v. 21, p. 551–560.

Ye, K., Cong, B., Hirajima, T., and Banno, S., 1999, Transformation from granulite to transitional eclogite at Haiyangsuo, Rushan County, eastern Shandong Peninsula: The kinetic process and tectonic implications: Acta Petrologica Sinica, v. 15, p. 21–36.

Ye, K., Yao, Y., Katayama, I., Cong, B.L., Wang, Q.C., and Maruyama, S., 2000, Large area extent of ultrahigh-pressure metamorphism in the Sulu ultrahigh-pressure terrane of East China: New implications from coesite and omphacite inclusions in zircon of granitic gneiss: Lithos, v. 52, p. 157–164, doi: 10.1016/S0024-4937(99)00089-4.

Zhang, R.Y., Hirajima, T., Banno, S., Cong, B., and Liou, J.G., 1995, Petrology of ultrahigh-pressure rocks from the southern Sulu region, eastern China: Journal of Metamorphic Geology, v. 13, p. 659–675.

Zhang, S., and Kang, W., 1989, The character of the blueschist belt and discussion of the formation age in central China: Journal of Changchun University of Earth Science, p. 1–9.

Manuscript Accepted by the Society 21 September 2005

Printed in the USA